1968

A study of swirling air flow in a converging nozzle

Charles William Lineberry

A STUDY OF SWIRLING AIR FLOW
IN A CONVERGING NOZZLE

BY

CHARLES WILLIAM LINEBERRY

A

THESIS

submitted to the faculty of

THE UNIVERSITY OF MISSOURI AT ROLLA

in partial fulfillment of the requirements for the

Degree of

MASTER OF SCIENCE IN MECHANICAL ENGINEERING

Rolla, Missouri

1968

Approved by

(advisor)

ABSTRACT

A study was conducted to determine the behavior of swirling air flow in a converging nozzle. Special instrumentation was constructed to obtain radial traverses of the flow at four axial positions. The data collected consisted of velocity, static pressure, and stagnation temperature.

The flow pattern demonstrated the Ranque-Hilsh effect and reversed axial flow in the core region. As the flow entered the nozzle, it had the characteristics of a free vortex. At the exit plane the characteristics were those of a forced vortex. The converging nozzle caused an increase in the magnitude of the axial velocity component.

ACKNOWLEDGEMENTS

The author wishes to thank the many persons that offered support and advice during the completion of this project.

Special graditude is expressed to Dr. L.G. Rhea. Had it not been for the time and effort spent by Dr. Rhea this accomplishment would not have been possible.

Also graditude is expressed to R.D. Smith for help received during the assembly and operation of the apparatus, and Professor A.V. Kilpatrick for offering his machining skills to produce a portion of the apparatus.

TABLE OF CONTENTS

	page
LIST OF ILLUSTRATIONS	v
LIST OF TABLES	vi
I. INTRODUCTION	1
II. REVIEW OF LITERATURE	3
III. DESCRIPTION OF APPARATUS	7
A. The Air Supply	7
B. The Vortex Generator and Nozzle	9
C. The Sensing Tubes and Support Mechanism	13
D. The Positioning Apparatus	19
IV. EXPERIMENTAL PROCEDURE	23
V. DISCUSSION OF RESULTS	27
VI. ERROR ANALYSIS	44
VII. CONCLUSIONS AND RECOMMENDATIONS	45
APPENDIX	50
Experimental Data	52
Calculated Data	56
Sample Calculations	60
BIBLIOGRAPHY	75
VITA	77

LIST OF ILLUSTRATIONS

Figure page

1. Photograph of Test Installation................. 8
2. Schematic Layout of Air Supply.................. 10
3. General Structure of Vortex Generator and Nozzle 11
4. Details of Sensing Tubes........................ 14
5. Support Mechanism............................... 17
6. Photograph of Support Mechanism and Sensing Tubes 18
7. Positioning Apparatus........................... 21
8. Element of Fluid................................ 27
9. Typical Velocity Distributions.................. 28
10. Total Velocity vs. Radius Ratio................ 29
11. Tangential Velocity vs. Radius Ratio........... 31
12. Axial Velocity vs. Radius Ratio................ 35
13. Static/Ambient Pressure Ratio vs. Radius Ratio. 37
14. Photograph of Streamlines at the Windows....... 39
15. Radial Velocity vs. Radius Ratio............... 40
16. Stagnation Temperature vs. Radius Ratio........ 43
17. Angular Positions.............................. 49
18. Nozzle Dimensions.............................. 51
19. Geometry of Support Mechanism.................. 62
20. Beam Geometry for Two Axial Stations........... 65
21. Beam Geometry for a Single Station............. 65
22. Geometry of Laser Support...................... 67

LIST OF TABLES

Table page

I. Experimental Data.......................... 52

II. Calculated Data............................ 56

III. Laser Positions........................... 68

I. INTRODUCTION

This thesis presents the results of an experimental study of swirling air flow through a converging nozzle. A similar study was made by Thompson (13) for values of radius ratio between zero and 0.6. The object of this work was to supplement the data collected by Thompson, and to provide velocity, static pressure, and stagnation temperature data corresponding to values of radius ratio between zero and 1.0.

A direct analytical approach to this problem involves solving the three dimensional, viscous, compressible flow equations. A solution of these equations requires simplifing assumptions which can only be substantiated from a thorough understanding of the flow pattern itself. To obtain this understanding it is only logical to resort to experiment.

Vortex flow of a gas produces effects not experienced in other flow patterns. The circular motion generates centrifugal forces in the fluid, and causes large velocity gradients which cause frictional effects to become an important factor. A particular characteristic of vortex flow is the Ranque-Hilsh effect. This effect is the separation of the gas stream into a core of low stagnation temperature and an annular region of high stagnation temperature. It is generally agreed that the

Ranque-Hilsh effect is caused by internal friction in the fluid, but complete agreement as to the mechanism of the temperature separation does not exist. Another characteristic is reversed axial flow in the core region. This is due to the low static pressure in the core.

Swirling flow in a nozzle has possible applications in the field of rocket propulsion. By utilizing the Ranque-Hilsh effect the stagnation temperature of the propellant could be raised. Another possible application is in thrust regulation. Inducing a component of swirl in the mass passing through a nozzle would decrease the axial velocity component, thus reducing the thrust. An even more sophisticated application, is to employ the centrifugal forces developed by the circular motion to remove the heavy uranium ions from the propellant of a nuclear rocket.

To date, the studies of vortex air flow have been confined to tubes. The results of these investigations are of some use in predicting the behavior of this type of flow in a nozzle, but would not be directly applicable in the design of such a nozzle.

II. REVIEW OF LITERATURE

The temperature separation in a gaseous vortex was first reported in 1931. G. Ranque, a french metallurgist, noticed the effect in connection with cyclone separators. He constructed and patented a device to duplicate the effect, hoping it could be employed as a refrigerator. Further investigation, however, indicated that the vortex motion was too inefficient as a refrigeration process, and this caused a loss of enthusiam. Interest was not renewed until 1946, when R. Hilsh published a paper relating his experience with the device.

Hilsh (6) constructed two vortex tubes of different radius and determined some of the variables affecting the performance. He found that inlet gas conditions, external pressure, and flow rate, all affect the degree of stagnation temperature separation within the tube. After examining the thermodynamic efficiency of the device he concluded that it was too low for practical use.

In a more recent study, J.E. Lay (8) conducted an experimental and analytical investigation to provide a better understanding of vortex flow in general. Pressure, velocity, and temperature traverses were taken at different axial positions along the tube. He compared this to a simple analytical model and found that as the flow progressed along the axis of the tube the influence of friction was to change the flow from a free to a forced vortex.

Savino and Ragsdale (11) studied a vortex generated within a right circular cylinder by means of guide vanes. Their experimental measurements indicated that the Ranque-Hilsh effect can be obtained without passing the flow through a long axial tube.

Keyes (7) measured properties in a vortex to determine the nature of the flow and the affect of important variables on the velocity profiles. He concluded that the most important parameters were the mass flow rate and the diameter of the tube.

Reynolds (10) presents data collected on a vortex tube with a blockage at the exit. The blockage eliminated the reversed flow common to all other experimental work. He found that the temperature separation occurs without reversed axial flow in the core.

Thompson (13) measured velocity and temperature distributions in the same flow system used in this investigation. He presents values of data for radius ratios from zero to 0.6 at three axial positions.

With the exception of Thompson's work (13), all experimental data have been collected by inserting relatively large probes into the flow. Since this creates disturbances that cannot be completely eliminated, all data must be somewhat suspect. All investigators have experienced the Ranque-Hilsh effect. Based on these previously published results, it may be concluded that the temperature separation is an inherent feature of the flow pattern.

The analytical work done in the vortex flow field is limited in application to the assumptions necessary to obtain solutions.

Donaldson and Sullivan (5) present solutions to the Navier-Stokes equations for different classes of vortex flow. Their solutions indicate that regions of reversed axial flow are possible.

Diessler and Perlmutter (4) analyzed the total temperature separation in vortex flow. They concluded that the stagnation temperature separation is due to the shear work done on the fluid as it traverses its spiral path.

Mager (9) arrived at solutions for swirling flow through a nozzle by assuming the flow frictionless. He indicates that the swirl would induce a void region along the axis of the nozzle which would restrict the area of the nozzle throat and offer some means of thrust regulation.

All previously discussed work concerned vortex flow of a compressible fluid. In 1956 Binnie and Hooking (3) conducted experiments with vortex water flow through a nozzle. Their findings did not produce any new conclusions pertinent to this report.

III. DESCRIPTION OF APPARATUS

The measurement of velocity and stagnation temperature in a gas stream requires the insertion of instrumentation into the stream. This obstruction causes distrubances which, if not minimized, can be detrimental to the results of such measurements. For this reason, the main consideration in the design of the following apparatus was to minimize this induced error.

The apparatus is classified and discussed in four main groups: A) the air supply, B) the vortex generator and nozzle, C) the sensing tubes and support mechanism, and D) the positioning apparatus. Figure 1 is a photograph of the test installation.

A) The Air Supply

To obtain appreciable velocities inside the nozzle, a large air supply was required. It was provided by two compressors operating in parallel. The compressors were an Ingersoll-Rand model 50-B and a Gardener-Denver model RS125A.

The discharge from the compressors was fed into a Worthington receiving tank, and from there, passed into the primary supply line of the vortex generator. An orfice type flow meter was placed in this line to measure the flow rate. The upstream pressure at the

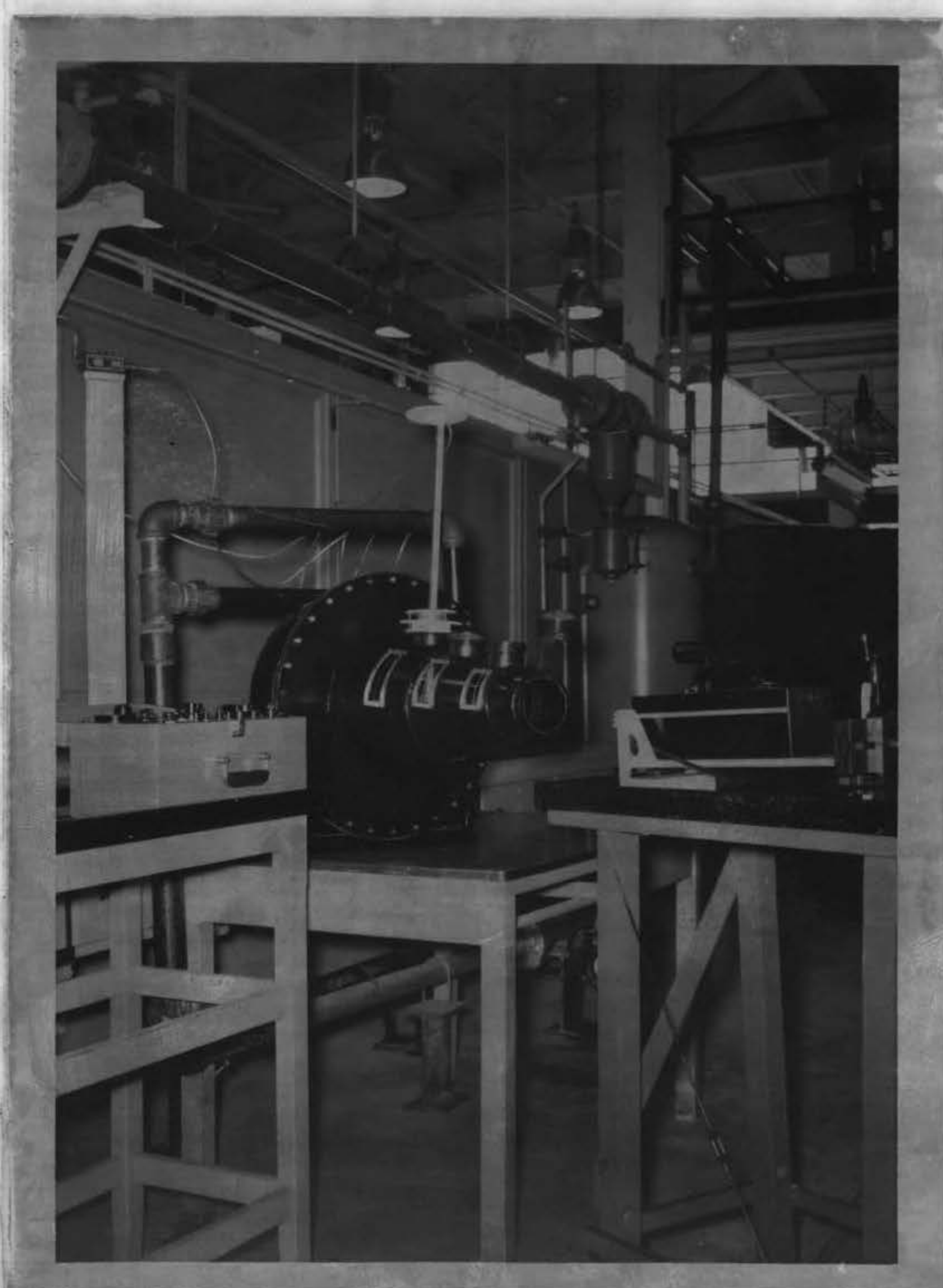

FIGURE 1. Photograph of Test Installation

orifice was measured by a U.S. pressure gage and the pressure difference across the orifice was indicated by a Meriam manometer model A-844 filled with mercury. The static temperature of the air in the primary stream was measured by an iron-constantan thermocouple placed in the primary supply line. A schematic layout of the air supply is shown in Figure 2.

B) The Vortex Generator and Nozzle

Figure 3 shows the general structure and internal characteristics of the vortex generator and nozzle. Two concentric sections of pipe formed the chambers of the vortex generator. The sizes were 20-in. O.D. and 14-in. O.D. Air entered the annular chamber formed by the pipes from the secondary supply lines. It was injected with a direction tangent to the inside surface of this chamber. Once in this region the air had an initial circular motion. From the outer chamber the air was forced through sixteen equally spaced guide vanes that were cut through the surface of the smaller pipe. In passing through the guide vanes a strong swirl was induced and a vortex resulted in the central region of the generator. From this point the swirling flow progressed through the converging nozzle which was mounted on the front of the vortex generator.

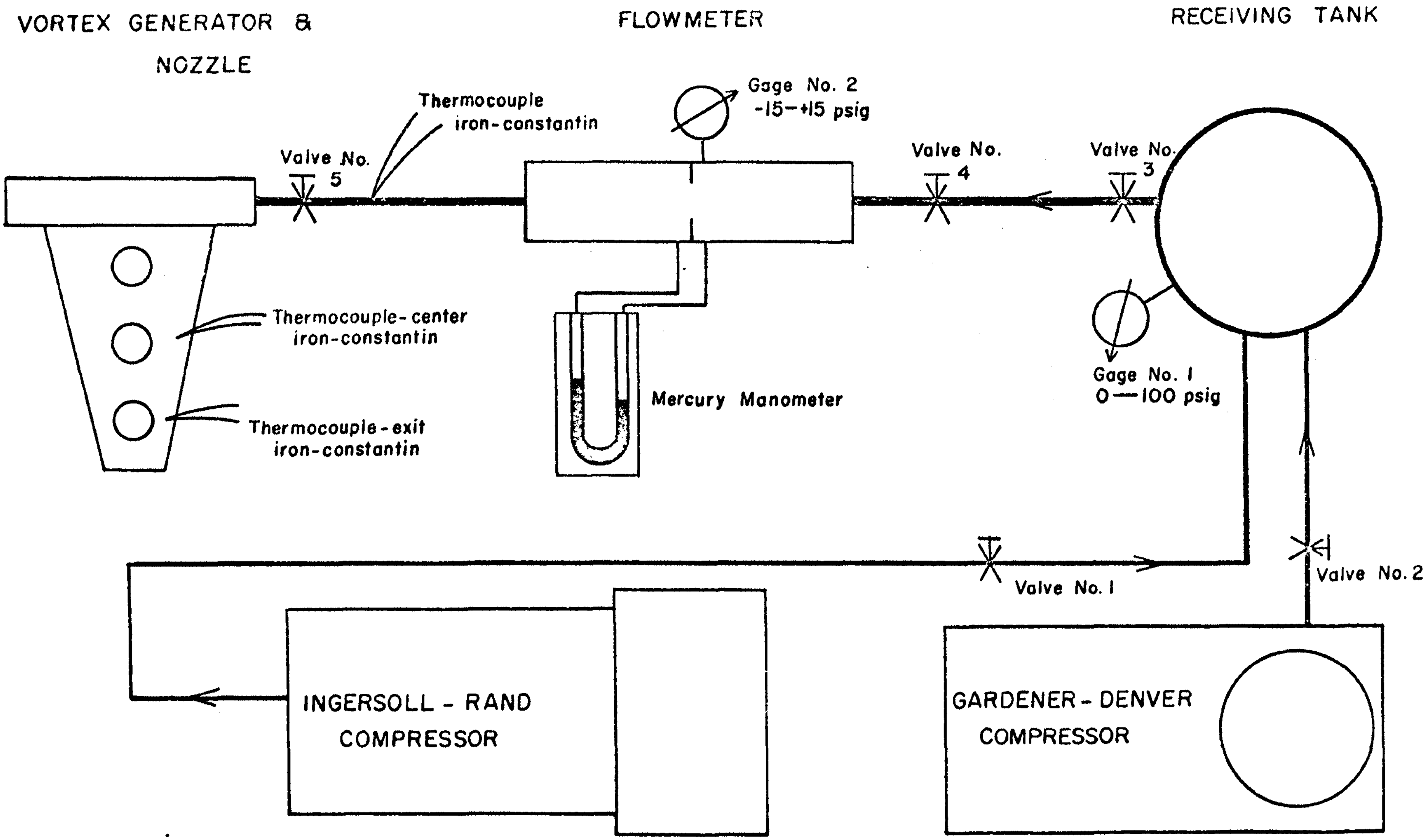

FIGURE 2. Schematic Layout of Air Supply

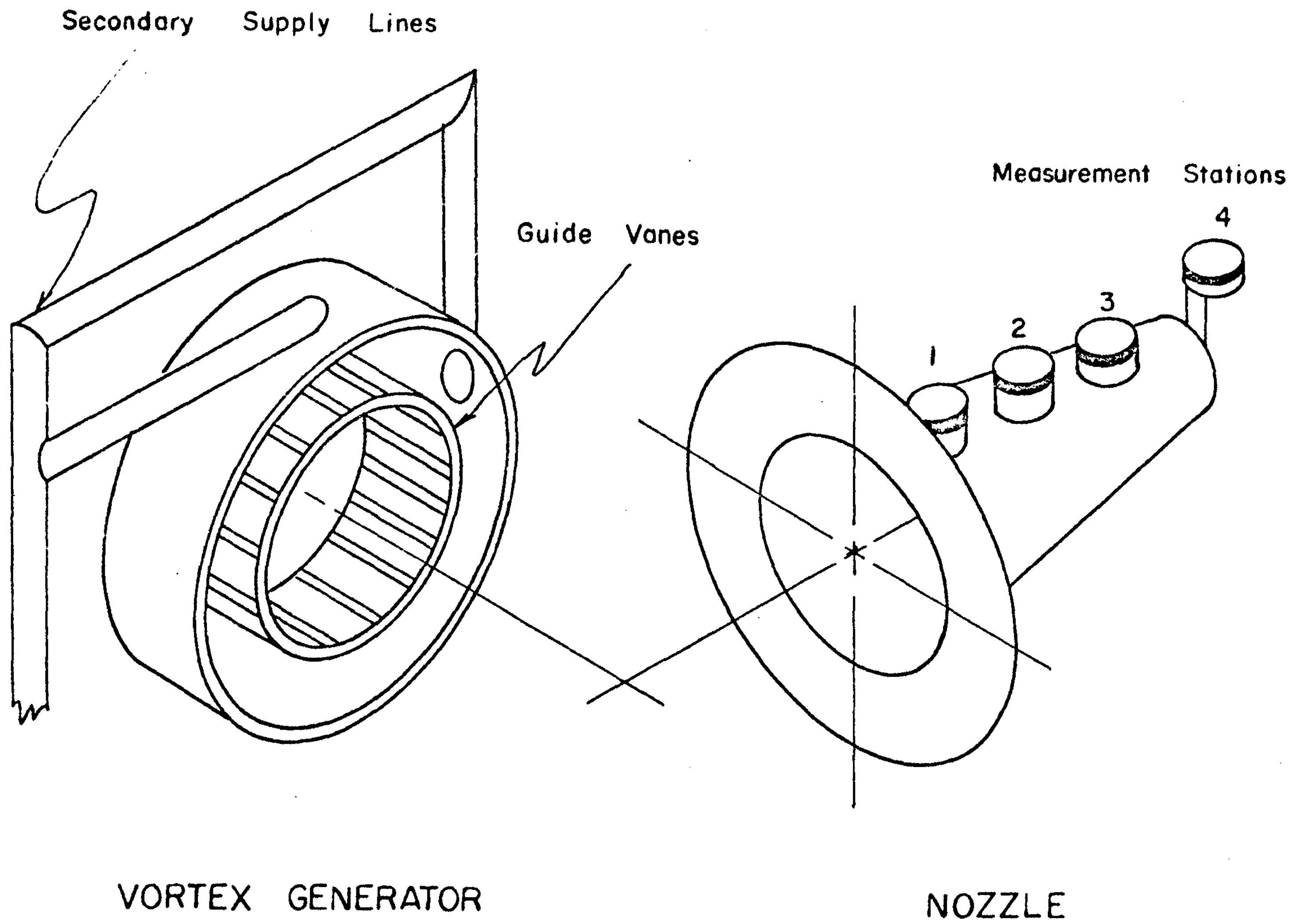

FIGURE 3. General Structure of Vortex Generator & Nozzle

The nozzle was conical in shape with inlet and exit diameters of 11 15/16-in. and 3 15/16-in. respectively. The total length from inlet to exit was 20 1/16-in. Located at three positions along the axis of the nozzle were measurement stations, which were simply short threaded sections of 2 1/2-in. O.D. steel pipe. These stations were fastened perpendicular to the axis of the nozzle, and served as support for the instrumentation. The spacing of the stations and all general sizes of the nozzle are given in the appendix, Figure 18. Two iron-constantan thermocouples were attached to the outside surface of the nozzle to indicate the heat loss to the atmosphere.

This portion of the apparatus was available from a previous investigation. It was constructed by S.A. Thompson for use in his research. For further information on the vortex generator and nozzle, refer to reference 13.

One modification made in the nozzle was the addition of three plexiglass windows. These were located at the three measurement stations to allow for visual positioning of the sensing tubes. Also, a fourth station was constructed at the exit plane to allow for the collection of data at this position.

C) The Sensing Tubes and Support Mechanism

A pitot tube and a stagnation temperature probe constituted the sensing probes. The pitot tube served to measure total and static pressure, and the stagnation probe was equipped with a copper-constantan thermocouple to indicate stagnation temperature. Details of both probes are shown in Figure 4.

The pitot tube was constructed of hypodermic needles. A small needle was placed inside a larger one to form the desired pressure chambers. Sizes of the pressure taps are shown in the figure. All lengths and sizes were within ASME requirements.

One unique characteristic of the pitot tube was the head to which it was fastened. The head was constructed of a small brass cylinder, and all parts threaded together. Liquid steel was used to seal the threads upon final assembly. Threaded joints were employed because of problems that developed in hot soldering the required seams. Besides forming the pressure chambers, the head contained hose connections for transmitting the pressures to a manometer. This manometer was a Meriam model 10BA10, filled with water.

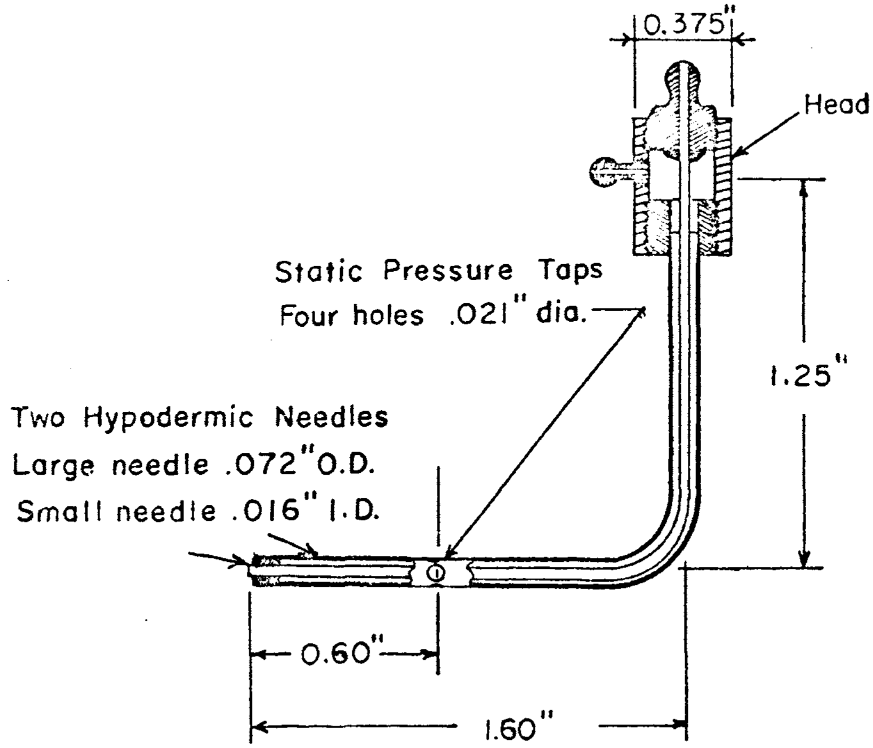

PITOT TUBE

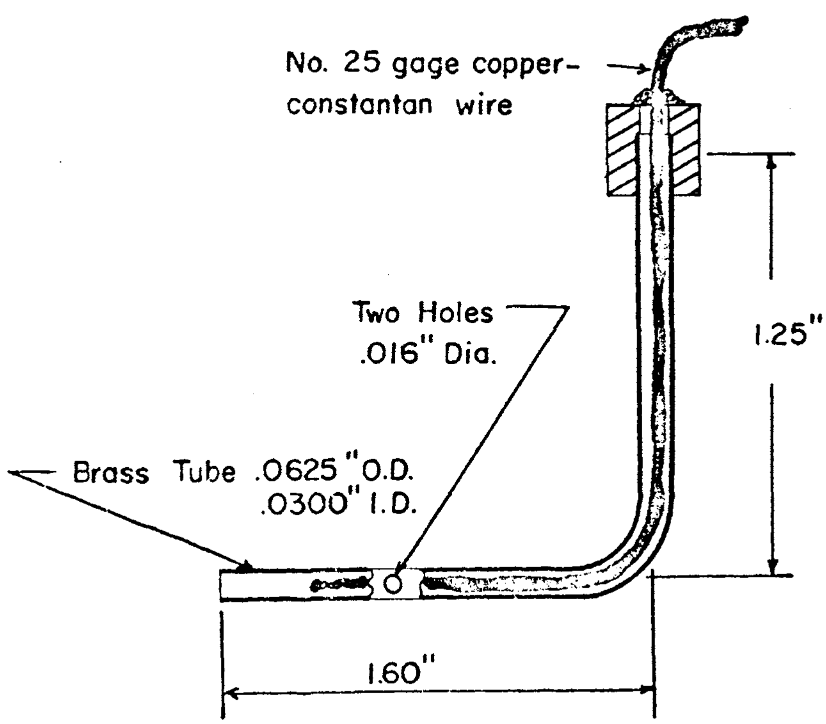

STAGNATION TEMPERATURE PROBE

FIGURE 4. Details of Sensing Tubes

After the pitot tube was assembled it was bent through a right angle. This was done in order that readings close to the wall could be obtained. It also eliminated disturbances near the measuring tip by placing the tip well below the support system.

The stagnation probe was fabricated from a section of small brass tubing. Two holes were drilled perpendicular to the axis of the tube to allow the stagnated air to leak off slowly, after coming nearly to rest around the thermocouple junction. Number 25 gauge copper-constantan thermocouple wire formed the measuring junction. A Honeywell model 2745 potentiometer, indicated the voltage at the junction. The length dimensions and shape of the stagnation probe were the same as those of the pitot tube.

Since the function of the pitot tube was to measure both the magnitude and direction of the velocity, it needed complete flexibility of position and direction. This was accomplished by developing a semirigid support mechanism.

The basis of support was a 2.5-in. diameter sphere. A system of brackets was constructed to mount the sphere at any desired measurement station with enough freedom to be partially rotated. A sectioned view of the mounting is shown in Figure 5, and a photograph of the actual system is shown in Figure 6. Two 1/4-in. O.D. aluminum tubes were mounted through the center of the sphere and passed down into the nozzle. These could be locked at any desired length by means of a set screw. In addition to serving as the basic support for the sensing probes, the aluminum tubes provided a means of transmitting the pressure lines and thermocouple wires, necessary for the operation of the sensing probes, out of the nozzle.

A small bracket that contained a mechanism for rotating the sensing tubes vertically was fastened to the bottom of the aluminum tubes. This mechanism contained a short section of 3/32-in. diameter shaft. The shaft had a small spur gear on one end, and threads on the other. The threaded end screwed into the head of the sensing tube to support it. A lock nut on the shaft prevented the sensing tube from working loose. By driving the spur gear with a matching worm gear the shaft could be rotated. This in turn rotated the sensing tube in a plane parallel to the support tubes. The worm gear was mounted on a 1/16-in. diameter steel rod that passed up through the sphere to allow the system to be operated from outside the nozzle. A pointer

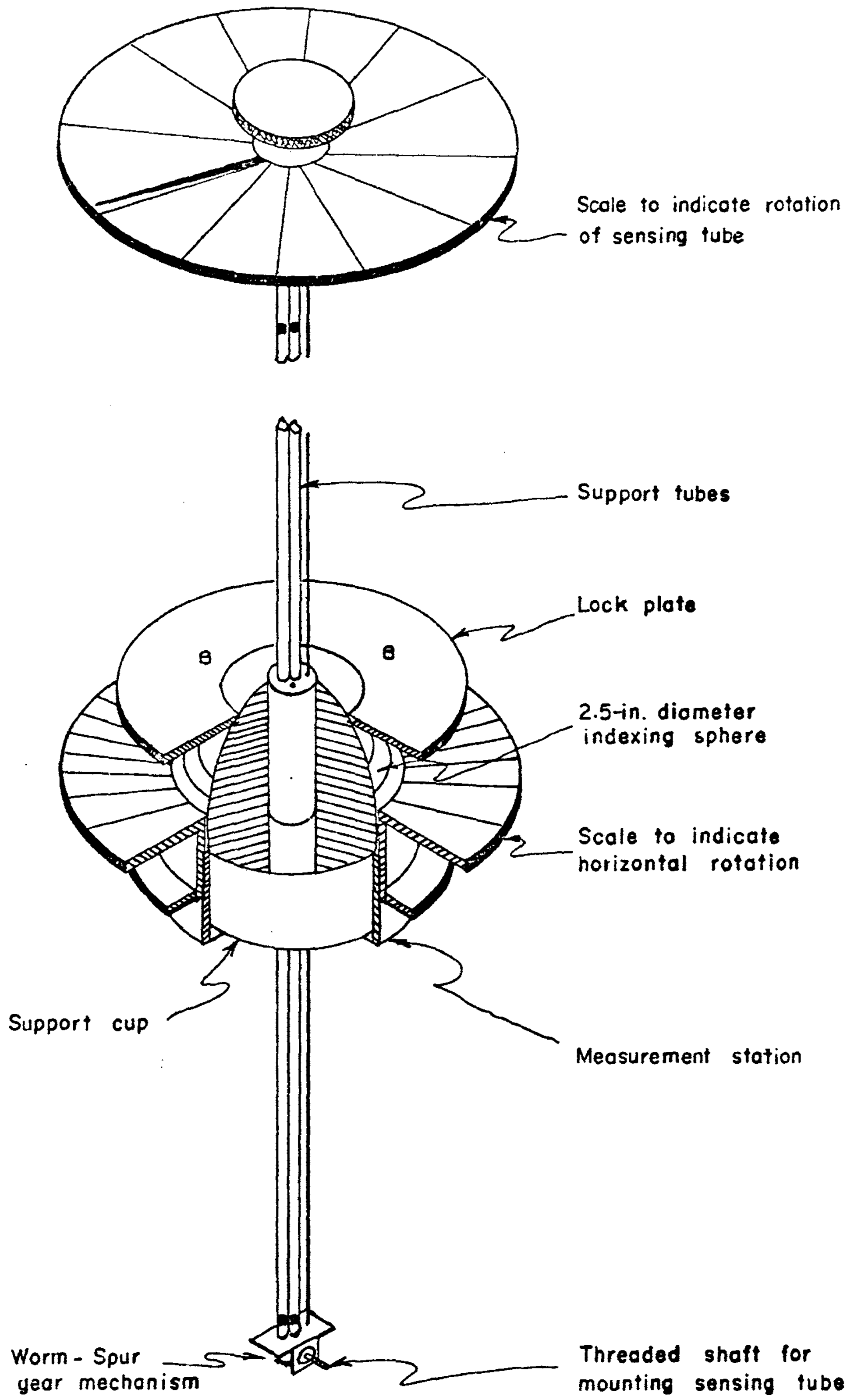

FIGURE 5. Support Mechanism

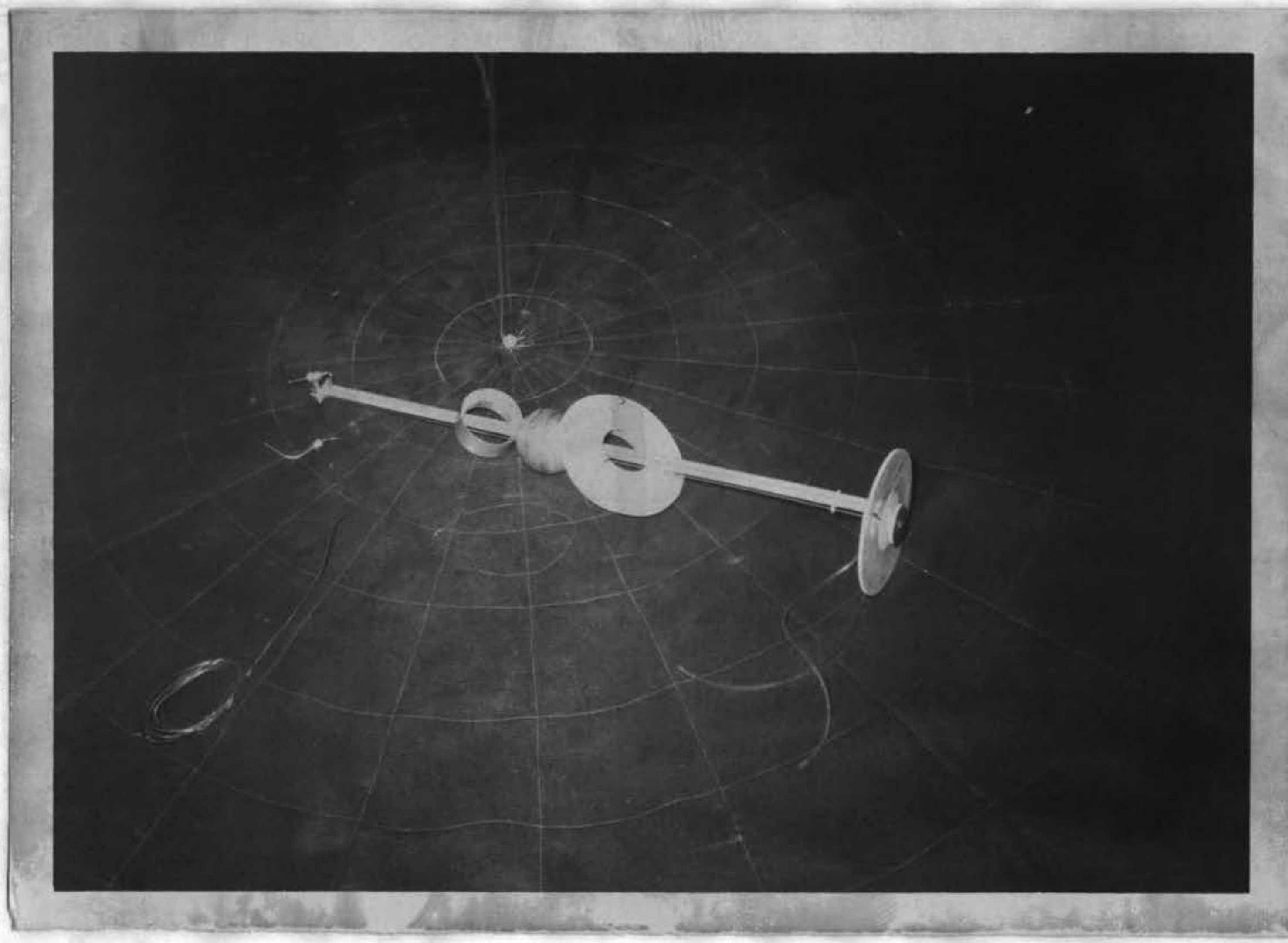

FIGURE 6. Photograph of Support Mechanism and Sensing Tubes

fastened to the shaft, and a scale calibrated in degrees were mounted at the top of the support tubes. This system allowed the inclination of the sensing tube with respect to the support tubes to be read directly.

The sphere was mounted in a cup of equal radius that fit inside the measurement station. A bracket with a horizontal scale calibrated in degrees threaded on the outside of the station. The sphere itself was graduated horizontally in one degree intervals. It also had one vertical line inscribed on its surface. The graduations allowed the angular positions of the support tubes to be read directly. These angular positions were needed to determine the direction of the flow at the tip of the pitot tube.

D) The Positioning Apparatus

To acquire related data at each axial station, it was necessary to make a radial traverse of the flow. This required readings at different radius ratios along a line of constant total radius. The flexibility of the instrumentation enabled any point to be obtained, but presented problems in maintaining the tip of the pitot tube at a desired point, while rotating it to sense the maximum flow direction. To overcome this difficulty, a visual positioning system was employed in which the tip of the pitot tube could be observed while its direction was being adjusted.

As mentioned previously, a plexiglass window was installed in the nozzle surface at each of the measurement stations. Circumferential lines 1/16-in. wide were painted on the inside surface of the nozzle, at each station, to indicate a plane perpendicular to the axis of the nozzle. This line allowed the operator to visually maintain the tip of the pitot tube in a plane of constant axial position. To locate the desired radial position, a Spectra-Physics laser model 130-C was mounted outside the exit of the nozzle. Its beam was directed into the nozzle, and its mounting enabled the beam to be shown through any desired radius ratio by tipping the laser through a predetermined angle. The system is shown in Figure 7. The laser support was constructed of plywood and consisted of a platform that pivoted about a line perpendicular to the beam. The system rotated by raising or lowering the rear of the support platform.

By visually maintaining the tip of the pitot tube in the beam and between the lines designating the desired axial plane, the operator could keep the pitot tube's tip at a desired point and sense for the direction

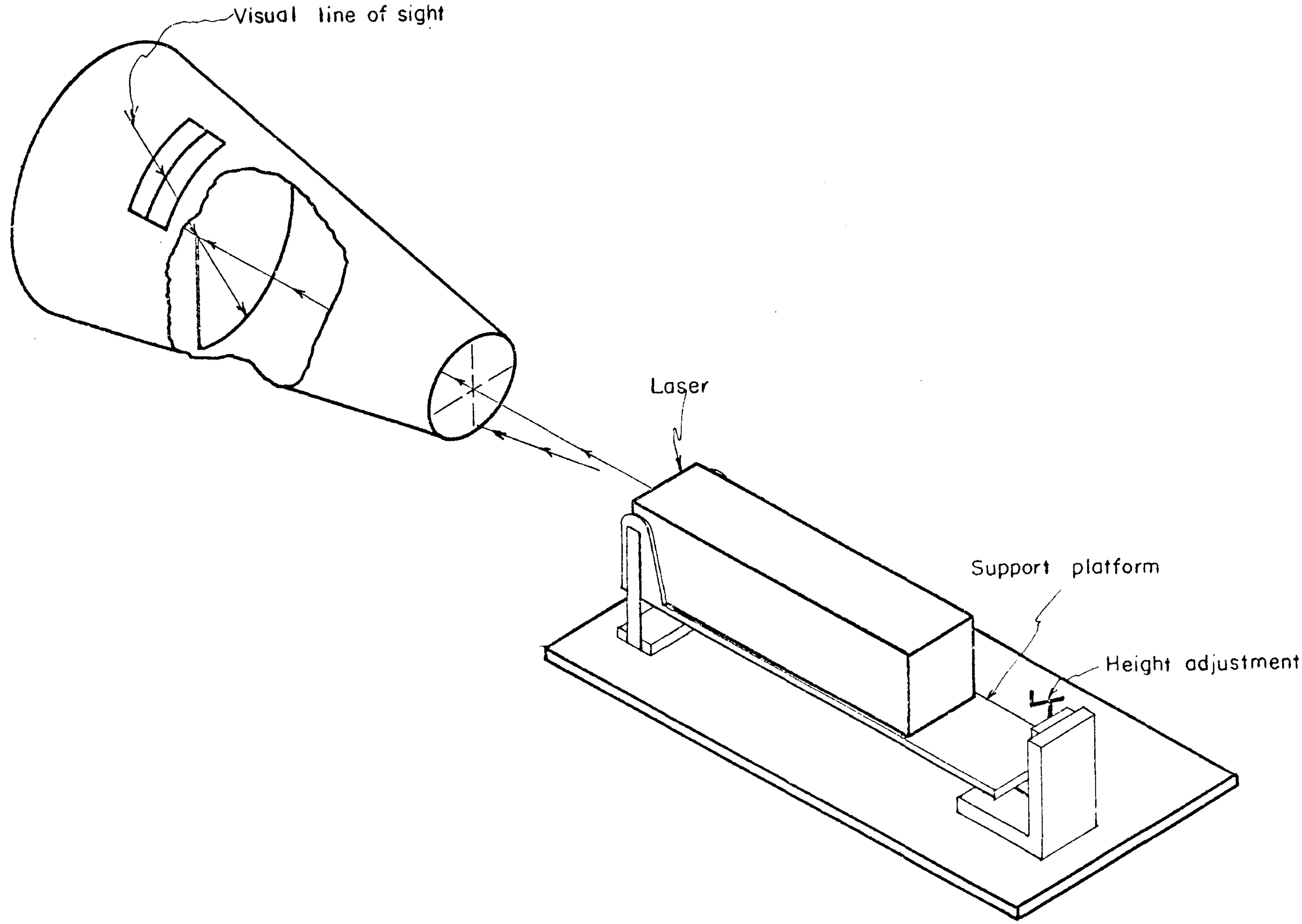

FIGURE 7. Positioning Apparatus

of the flow. The positioning system allowed the data points to be located within ± 1/16 in.

IV. EXPERIMENTAL PROCEDURE

The General Electric motor-generator set was started to provide power for the prime mover of the Ingersoll-Rand compressor and the cooling water pump. After the water pump was primed and started, all air valves were opened and the compressors were started. Valve no. 3, Figure 2, was then adjusted until the maximum flow rate was indicated at the orifice. The system was then allowed to run until it reached steady flow conditions.

Steady-state was indicated by the thermocouples that were attached to the outside surface of the nozzle. Assuming the convection coefficent of the nozzle surface did not change, steady-state was taken as the condition when the surface temperature reached a constant value.

The pitot tube was threaded and locked on the support mechanism, and all scales were adjusted to give their zero readings. Beginning at station one, the instrumentation was mounted and the radial traverses were begun. Readings were started at the wall, so that the initial position of the laser beam was parallel to the inside surface of the nozzle. With the tip of the pitot tube at the desired point, the system was rotated and tipped until a maximum velocity was indicated. The sphere was then locked in position and the data were recorded. The values recorded were, (1) the magnitude of the velocity, (2) the horizontal rotation of the support tubes, (3) the vertical inclination of the support tubes, and (4) the inclination of the pitot tube with respect to the support tubes. After the velocity and position were recorded, the total pressure side of the manometer was opened to the atmosphere. This procedure gave the value of local static pressure by comparing it with atmospheric. The pressure difference was then recorded and the system was set for the next data point.

Successive data points were obtained by changing the angle of the laser and repeating the previous procedure. The readings were started at the wall and progressed to the center of the nozzle. Velocity traverses were taken at three internal stations and at the exit plane of the nozzle. Only five data points could be obtained at the exit plane, because the lower end of the support tube caught on the lip of the nozzle exit and made the center points inaccessible.

The velocities were initally obtained, and then checked in a second run. It should be noted here that during the second run of the third and fourth stations, and during the collection of the stagnation temperatures, the orfice manometer was out of service. The upstream pressure was the same as in the first run, but the differental across the orifice was not available. Therefore, it was necessary to assume that the flow rate in the second run was the same as in the first. This assumption seems valid since the internal velocities measured in the two different runs corresponded.

Once all desired velocities were measured, the pitot tube was replaced by the stagnation temperature probe. By returning to the recorded positions the corresponding stagnation temperatures were obtained. When reading the values of stagnation temperature, the laser was disconnected in order that any heating by the light would be eliminated.

After all data were collected, some flow visualization was performed. Due to the low pressure in the receiving tank, the Gardener-Denver compressor was losing oil through its separator. The oil was carried into the nozzle and presented a nuisance during the collection of data, but it did provide flow visualization at the windows. The circular flow caused the heavy oil to be immediately thrown onto the inside surface of the nozzle. It formed the streamlines at the wall which showed up quite well on the plexiglass windows. Finely ground chalk was injected into the vortex generator to allow these streamlines to be photographed.

V. DISCUSSION OF RESULTS

The experimental data are presented in Figures 10 - 16. The variables are plotted versus the dimensionless radius for ease of comparison.

Figure 10, presents the total velocity distributions at the four axial positions. A comparison of the total velocity distributions to their respective tangential velocity distributions, Figure 11, shows that the two are similar in both shape and magnitude. This comparison indicates that the tangential velocity is the dominating component, and in this case was the determining factor in the behavior of the flow.

The general trend of the tangential velocity was to increase from the wall to a maximum value, and decrease from there to the core. To explain this trend, consider a simple element of frictionless fluid moving with a circular motion, Figure 8.

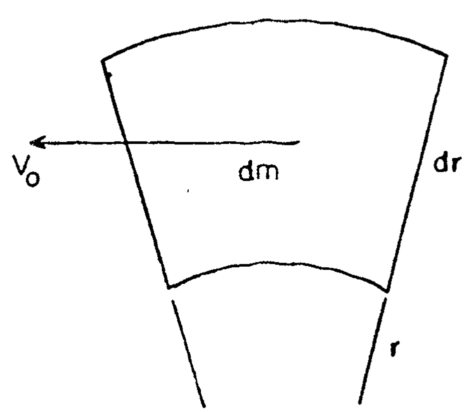

FIGURE 8. Element of Fluid

The angular momentum may be written as $\Sigma T = (dm)\frac{d(rV_\theta)}{dt}$.

Since friction is neglected $\Sigma T = 0$.

Therefore, $0 = (dm)\frac{d(rV_\theta)}{dt}$ or $d(rV_\theta) = 0$

Integrating this expression yields, rV_θ = constant or $V_\theta = \frac{C}{r}$.

This expression indicates that the tangential velocity of a frictionless fluid is a hyperbolic function of radius. A velocity distribution as shown in Figure 9a, would result from this type of motion. It would approach zero at large radius, and would be infinate at the center. The experimental distributions indicate and increase of this type from the wall, but deviate when the point of maximum velocity is reached.

Next consider a fluid moving in a circular path with friction dominating the flow. The friction causes the fluid to move with a rotation similar to a rigid body i.e.(with a constant angular velocity). This yields a tangential velocity with $V_\theta = \omega r$.

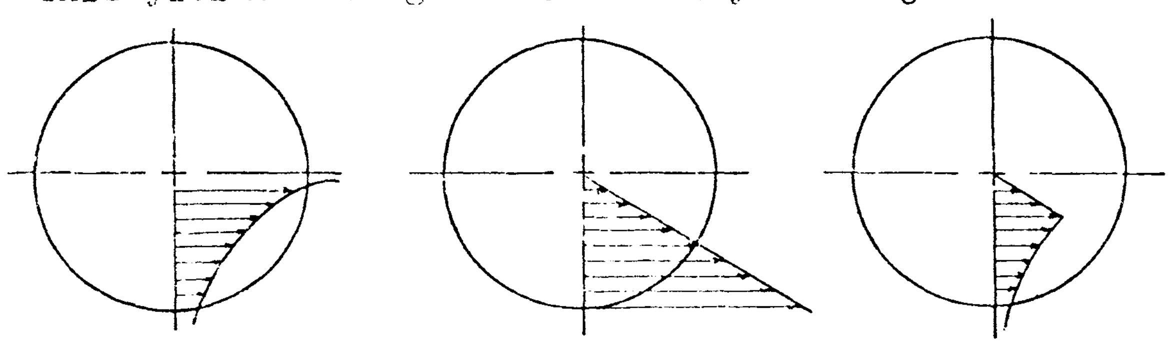

a. frictionless b. frictional c. combination

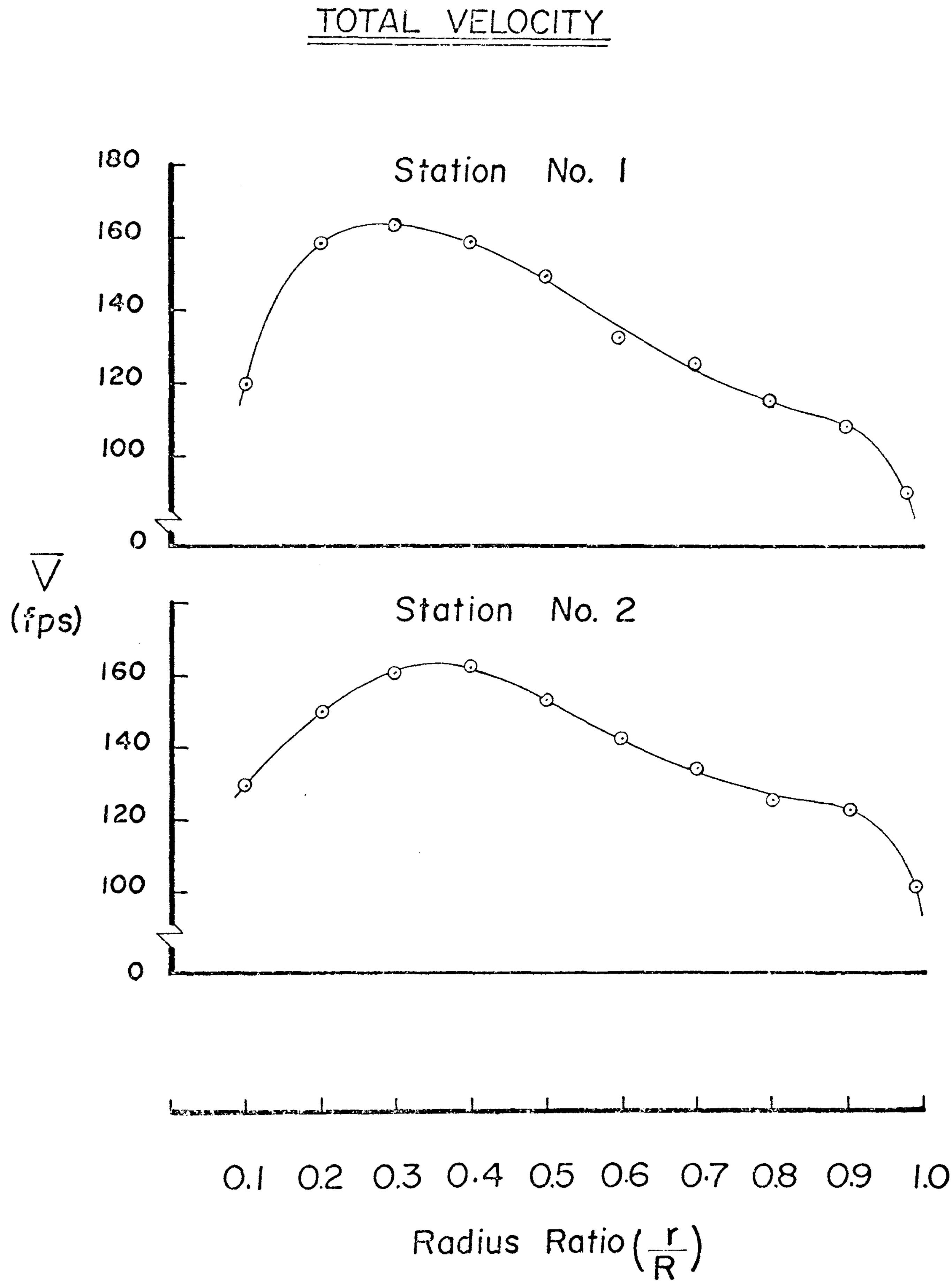

FIGURE 10. Total Velocity vs. Radius Ratio

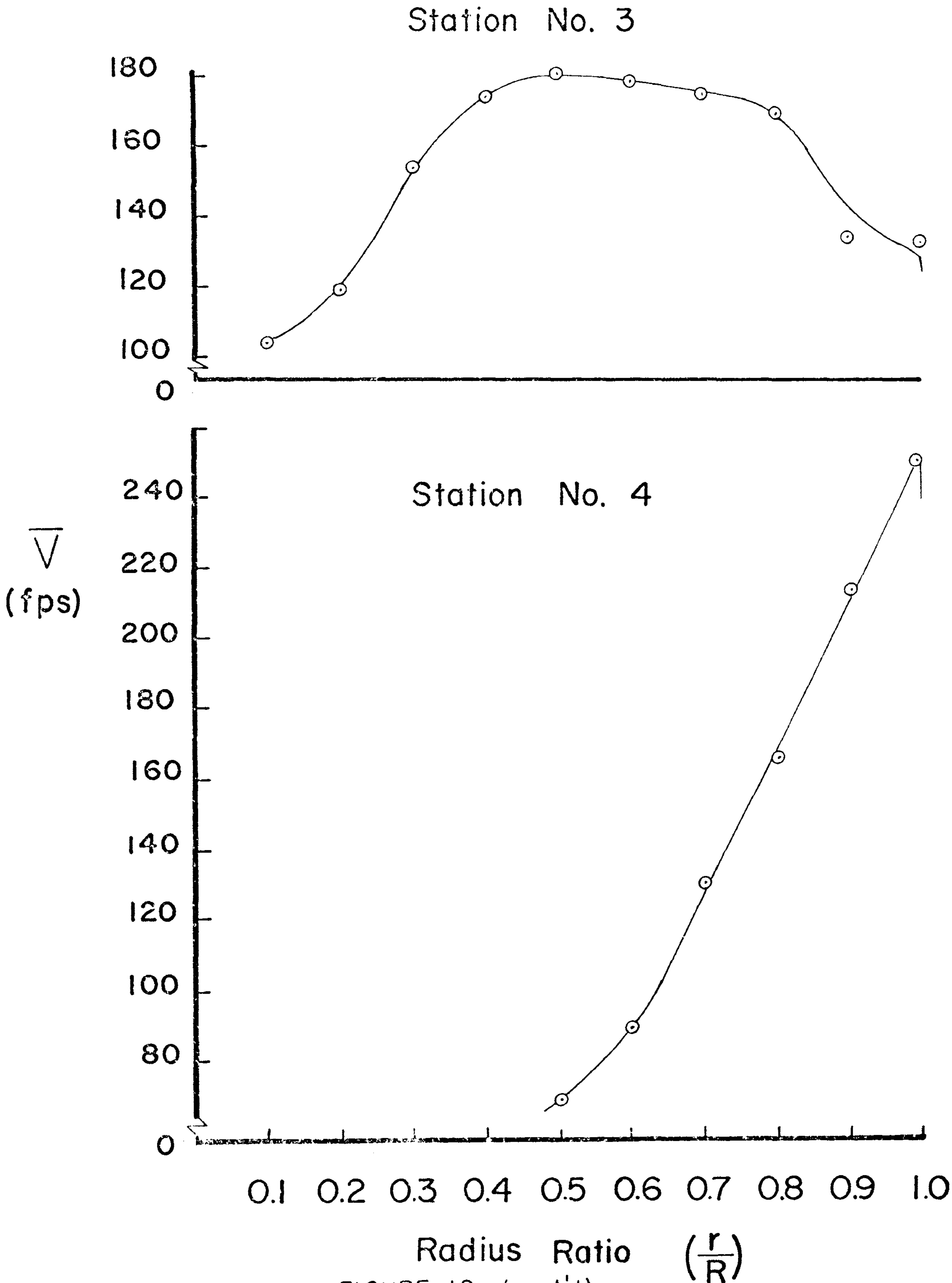

FIGURE 10. (cont'd)

TANGENTIAL VELOCITY

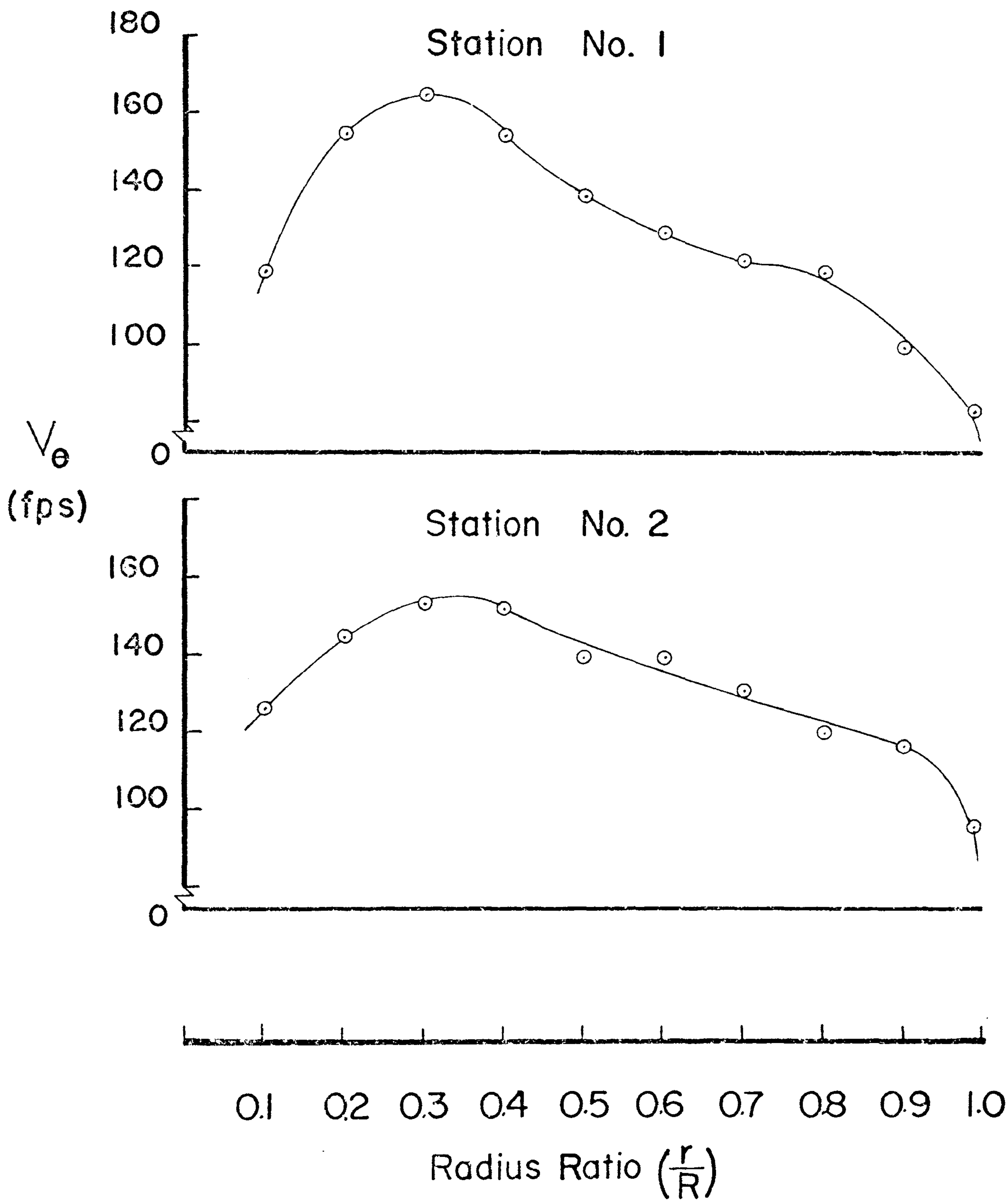

FIGURE 11. Tangential Velocity vs. Radius Ratio

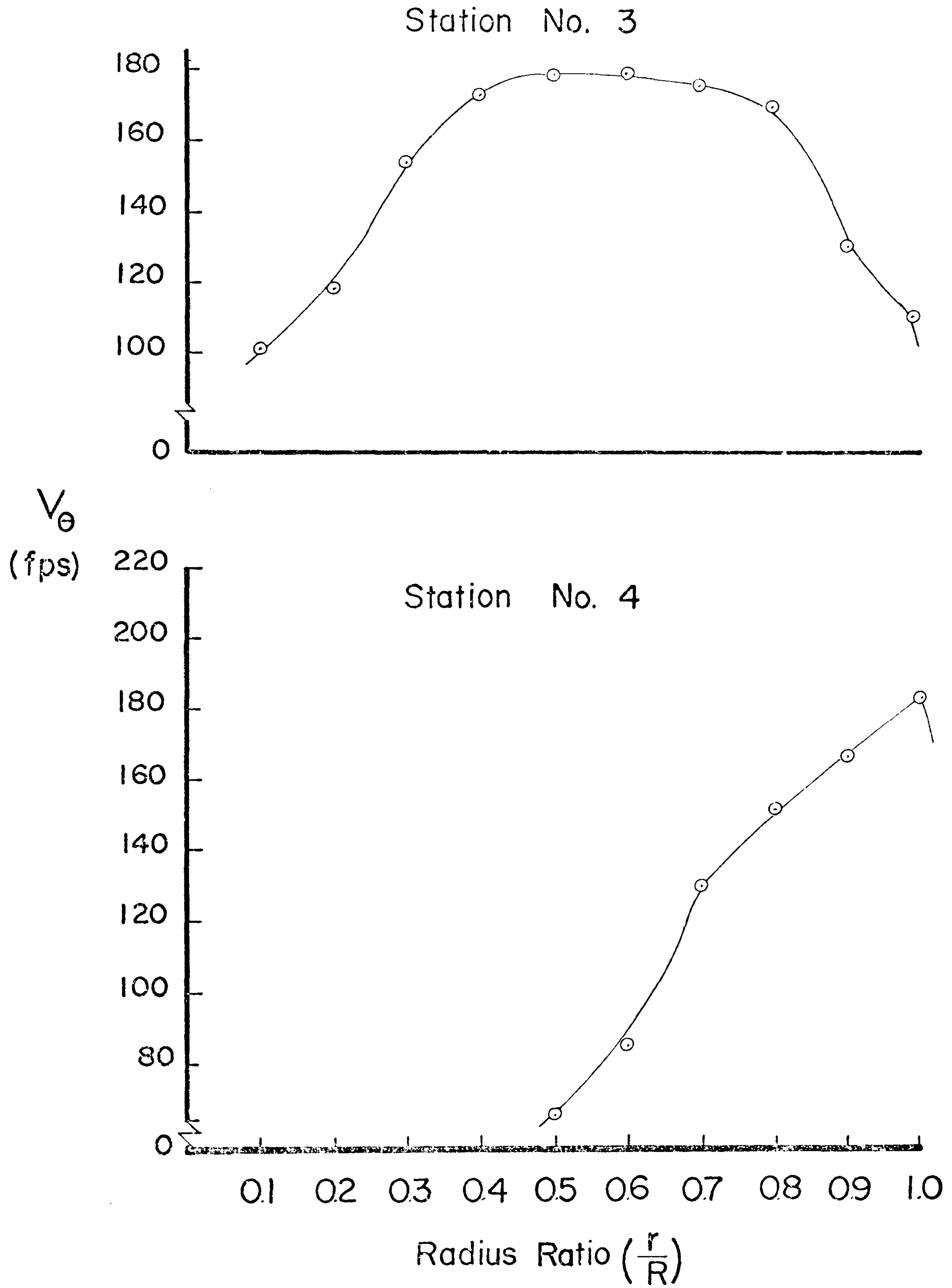

FIGURE 11. (cont'd)

A distribution of this type is shown in Figure 9b. Comparing the frictional motion to the experimental tangential velocity distributions, it can be seen that the experimental results indicate a motion similar to this in the center region.

This analysis would indicate that the actual tangential velocity distributions are a combination of the two preceding types, Figure 9c, or that friction is the dominating factor in the center of the vortex and is negligible in the outer region.

The axial change in the tangential velocity indicates that as the flow progresses through the nozzle, friction becomes more dominant. That is, upon entry a small region in the center is moving with wheel type flow, but as the axial position increases, a larger portion of the fluid is moving in this manner. At the exit plane the tangential velocity is practically linear with radius and the maximum velocity occurs near the wall.

A tangential distribution of this nature also complies with angular momentum requirements. As the fluid enters the vortex generator, it is given a specific angular momentum. The torque on the fluid due to friction will tend to dissipate this momentum. Upon entry, the frictional torque has not affected the flow considerably, so the mass near the center of the vortex must move with a greater velocity to conserve its angular momentum. As the fluid moves through the vortex, the viscous forces tend to distribute the momentum of the high velocity region to the slower moving outer region. This will cause an increase in the velocity of the fluid in the outer region, and will cause the tangential velocity distributions to change accordingly.

Examination of the axial velocity distributions, Figure 12, reveals a region of reversed axial flow in the core of the vortex. This is induced by the low static pressures in the center, Figure 13. The low static pressures correspond to the high velocities. Near the entrance of the nozzle, the maximum velocity occurred near the center. As the fluid moves toward the exit, the velocities increase due to the area change and the static pressures decrease accordingly.

The axial distributions at the third and fourth stations indicate an outward flow at the very center of the nozzle. Since the data points at the center of the exit plane were not available, this characteristic can be substantiated by considering the total mass flowing

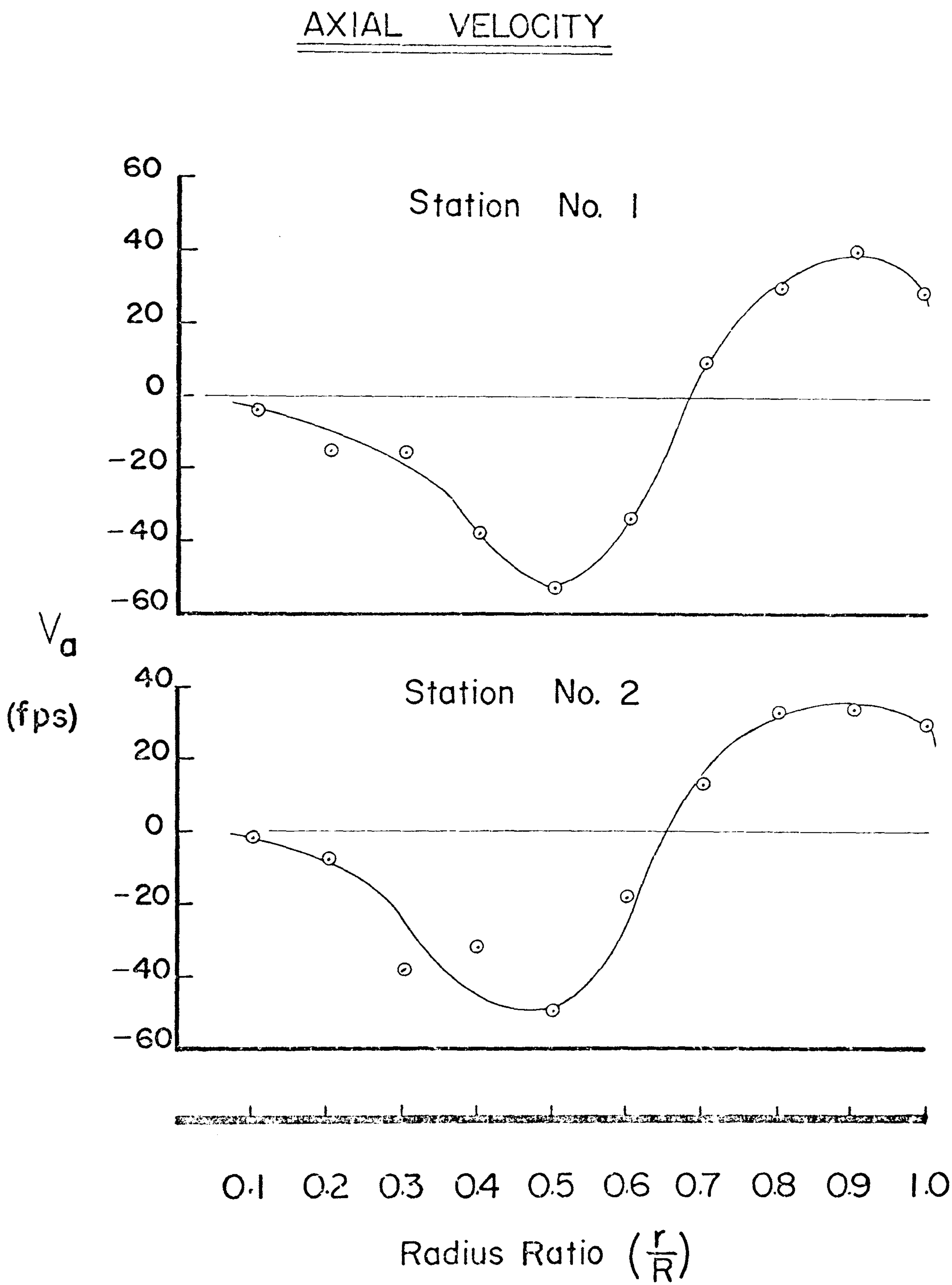

FIGURE 12. Axial Velocity vs. Radius Ratio

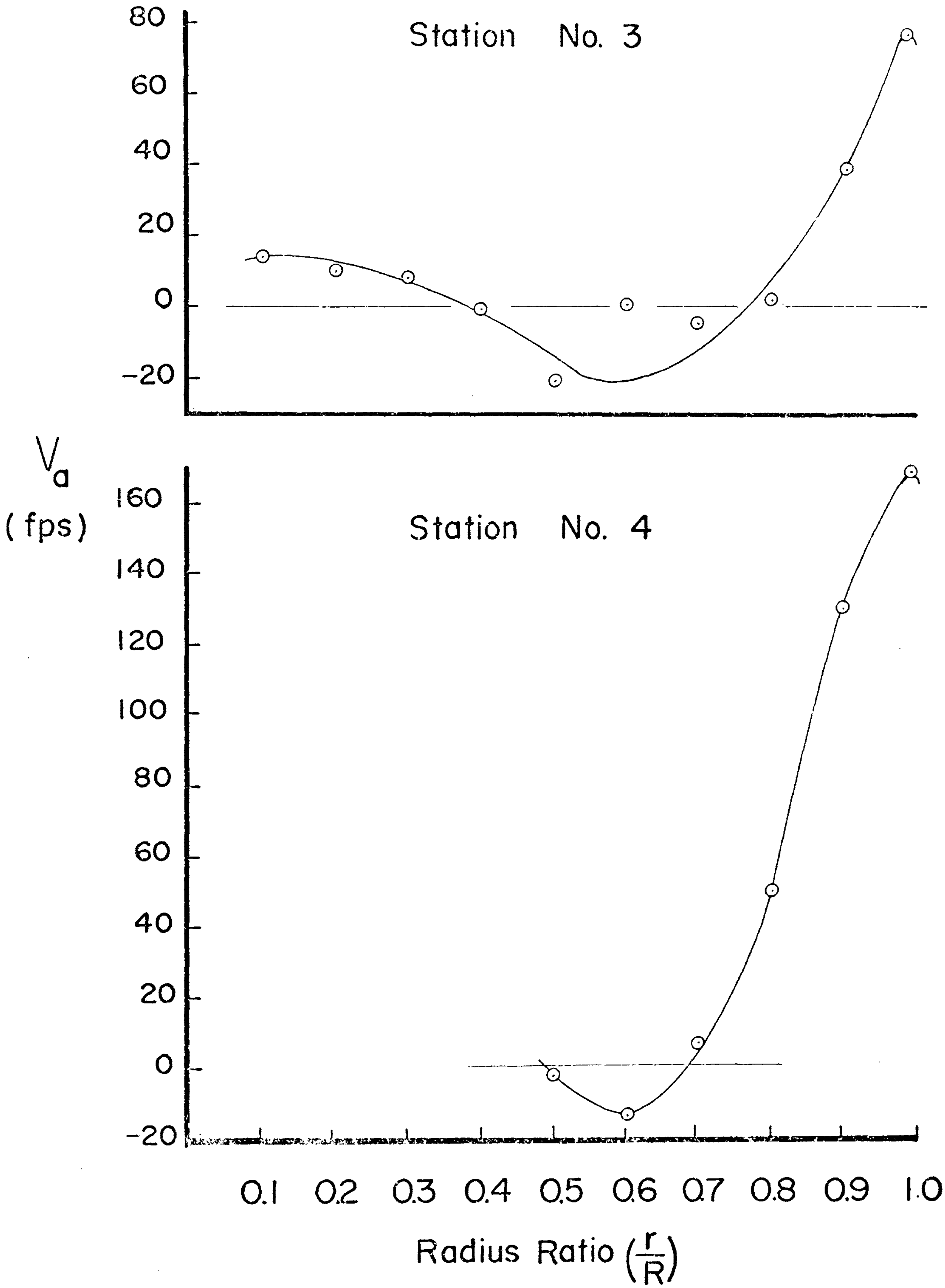

FIGURE 12. (cont'd)

STATIC — AMBIENT PRESSURE

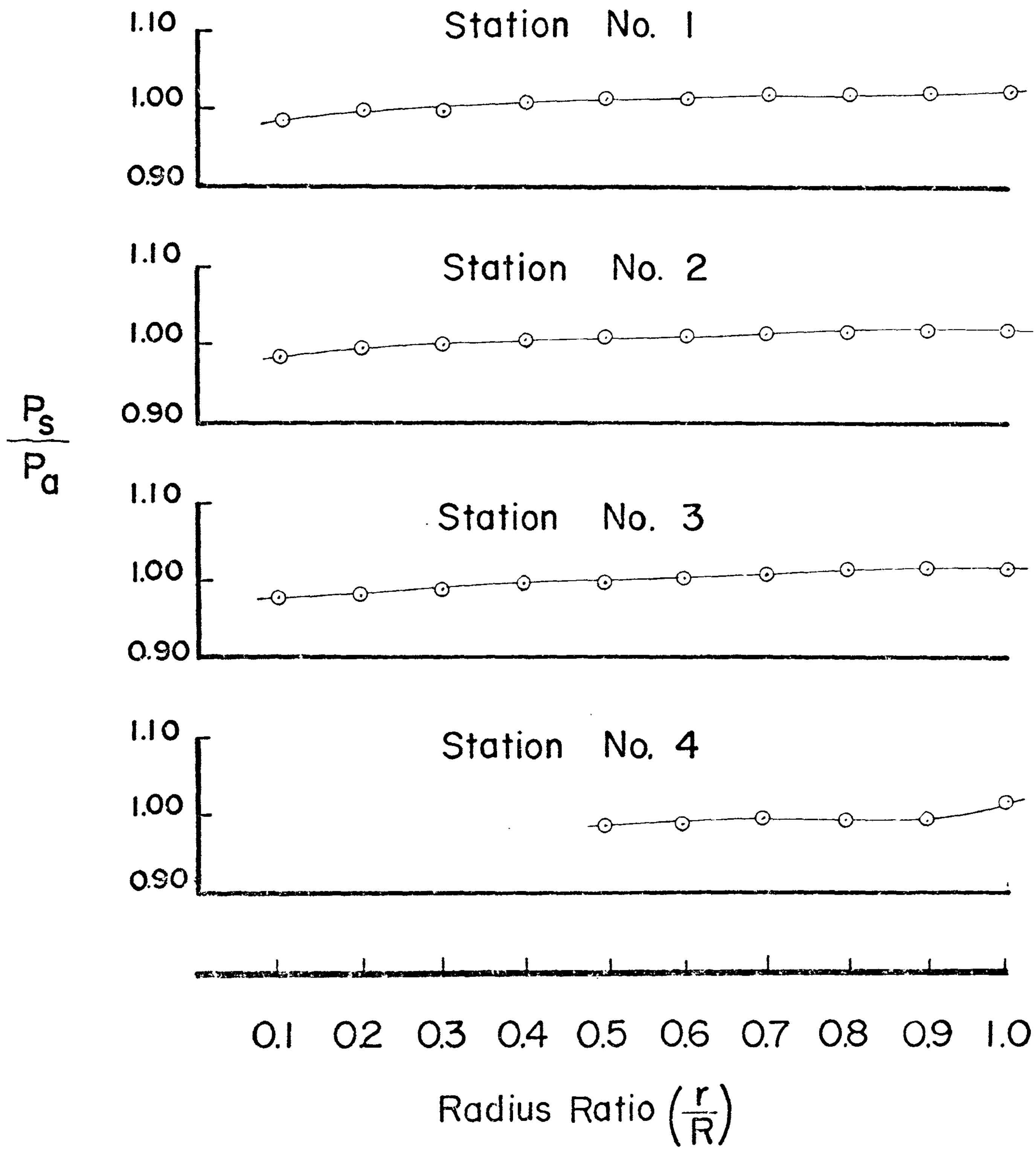

FIGURE 13. Static-Ambient Pressure Ratio vs. Radius Ratio

through the system. The mass leaving the system through the annular region near the wall at the exit plane, can be calculated by integrating the axial velocity distribution over the region indicating outward flow. This procedure is shown in the appendix. The value of mass flow rate obtained was 0.247 lb_m/sec. The mass flow rate into the system from the air supply was 0.287 lb_m/sec. Since the system was operating at steady state conditions, the excess mass must be leaving the system through the center of the exit plane. This means that the axial velocity at the center of the exit plane has an outward direction.

Figure 14, is a photograph of the streamlines at the windows of the nozzle. As can be seen, the flow angle increases with increasing axial position. Previous flow visualization in a plexiglass tube of constant radius (8), did not reveal any appreciable changes in the flow angle. These results indicate that there was an increase in the axial velocity component due to the convergence of the nozzle.

Radial velocity tended to increase from the center of the vortex to a maximum value, and then decrease from there to the wall, Figure 15. Except at the wall the radial velocities are away from the center line.

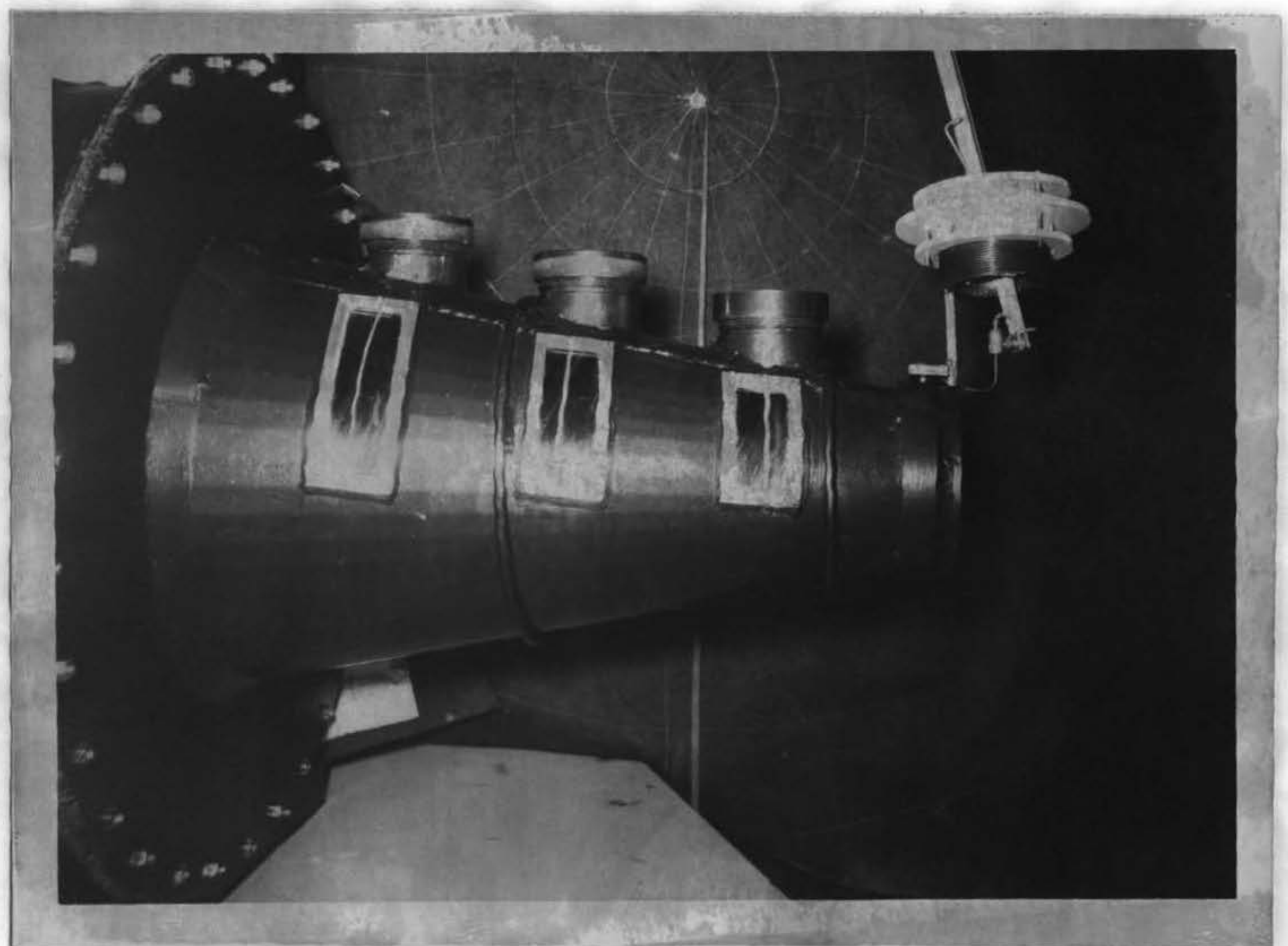

FIGURE 14. Photograph of Streamlines at the Windows

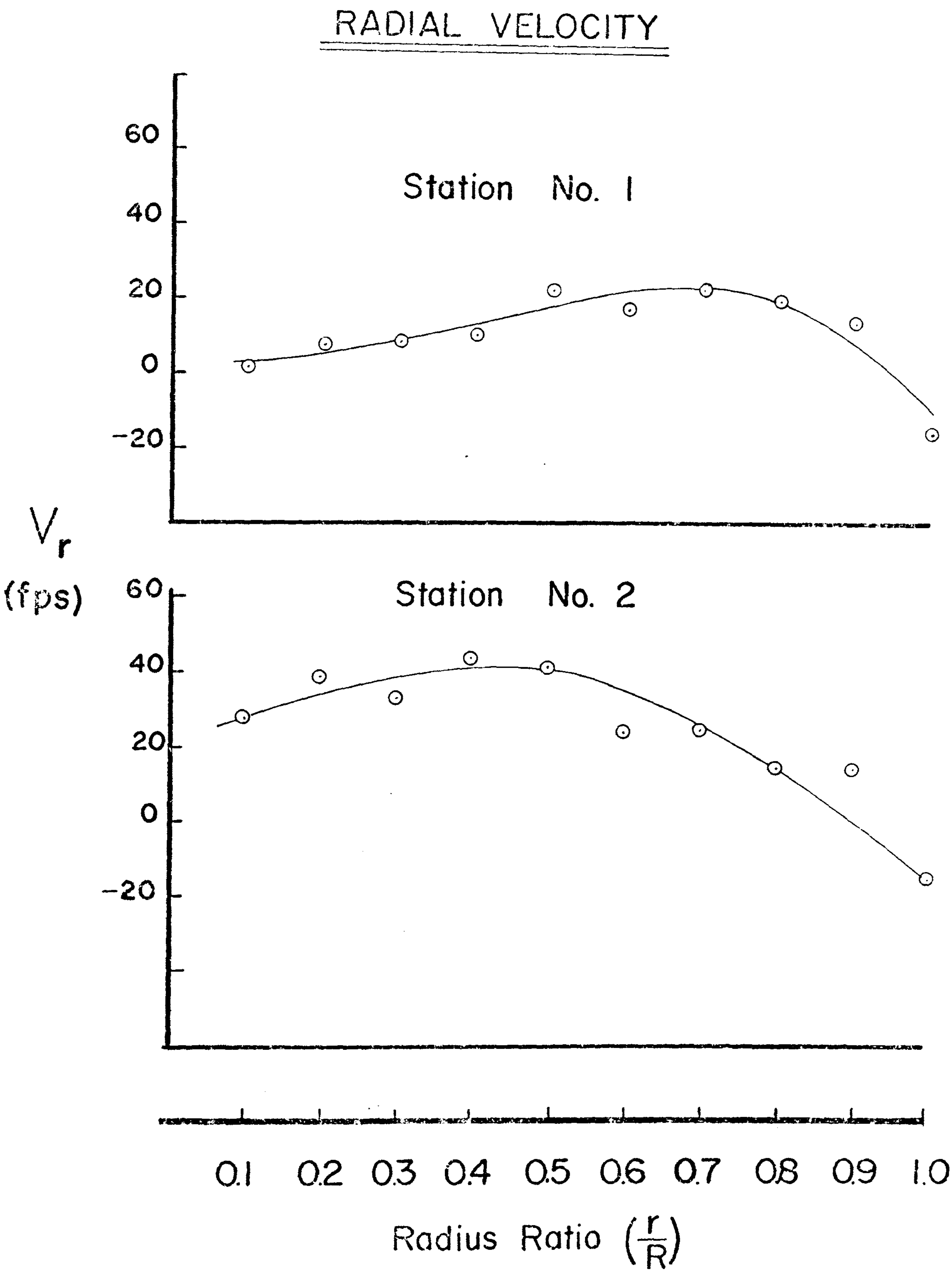

FIGURE 15 Radial Velocity vs. Radius Ratio

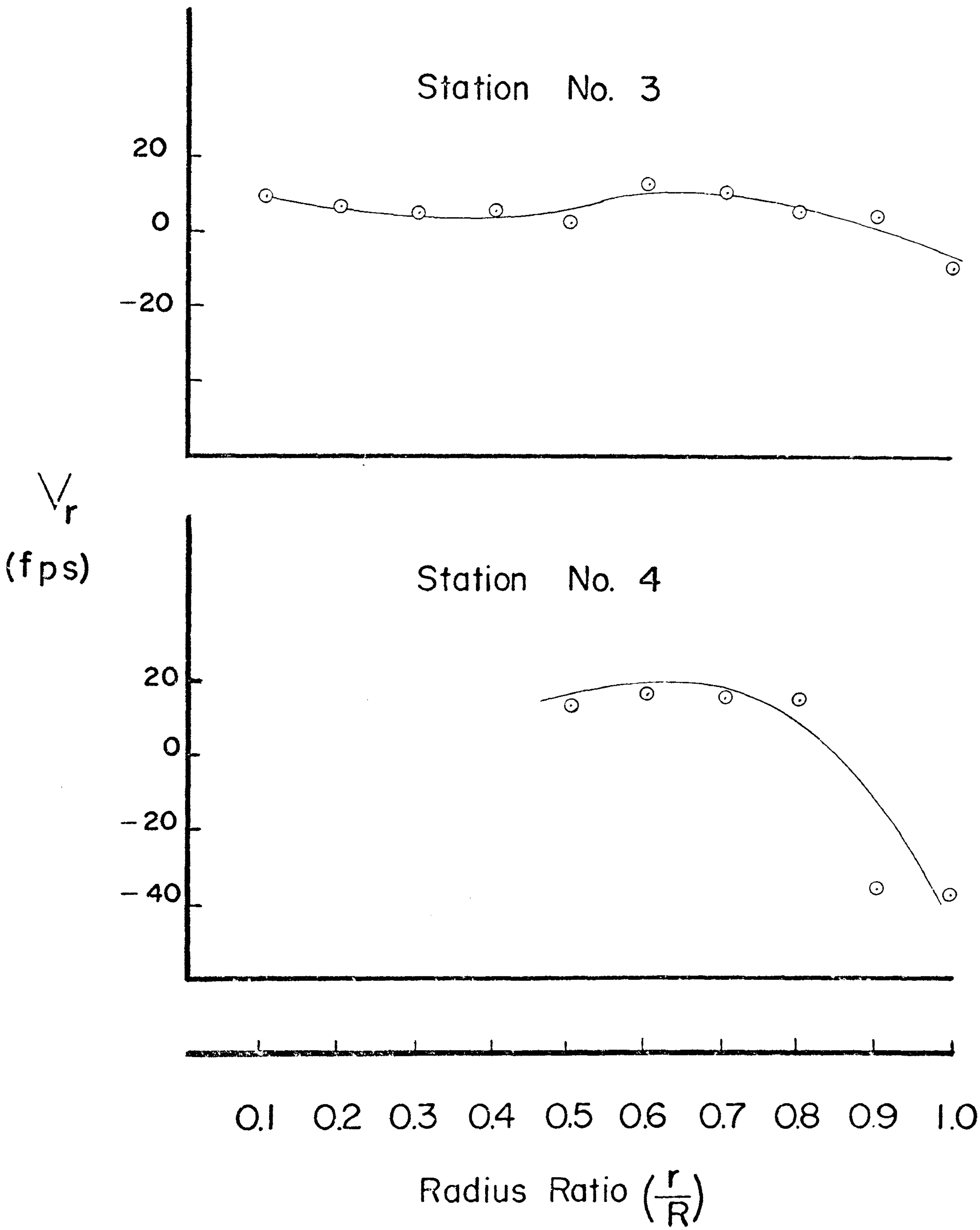

FIGURE 15. (cont'd)

the nozzle. The values at the wall are inward in that the flow is moving in a path parallel to the wall of the converging nozzle.

As the flow progressed through the nozzle, the main effect on radial velocity was to decrease its magnitude. This might be attributed to decreasing centrifugal forces due to decreasing total radius.

The stagnation temperature distributions, shown in Figure 16, indicate that the Ranque-Hilsh effect existed. At station one, the stagnation temperature was nearly constant. The remaining stations indicate a separation of approximately eight degrees Rankin The overall loss in stagnation temperature can be attributed to heat transfer from the nozzle surface to the atmosphere.

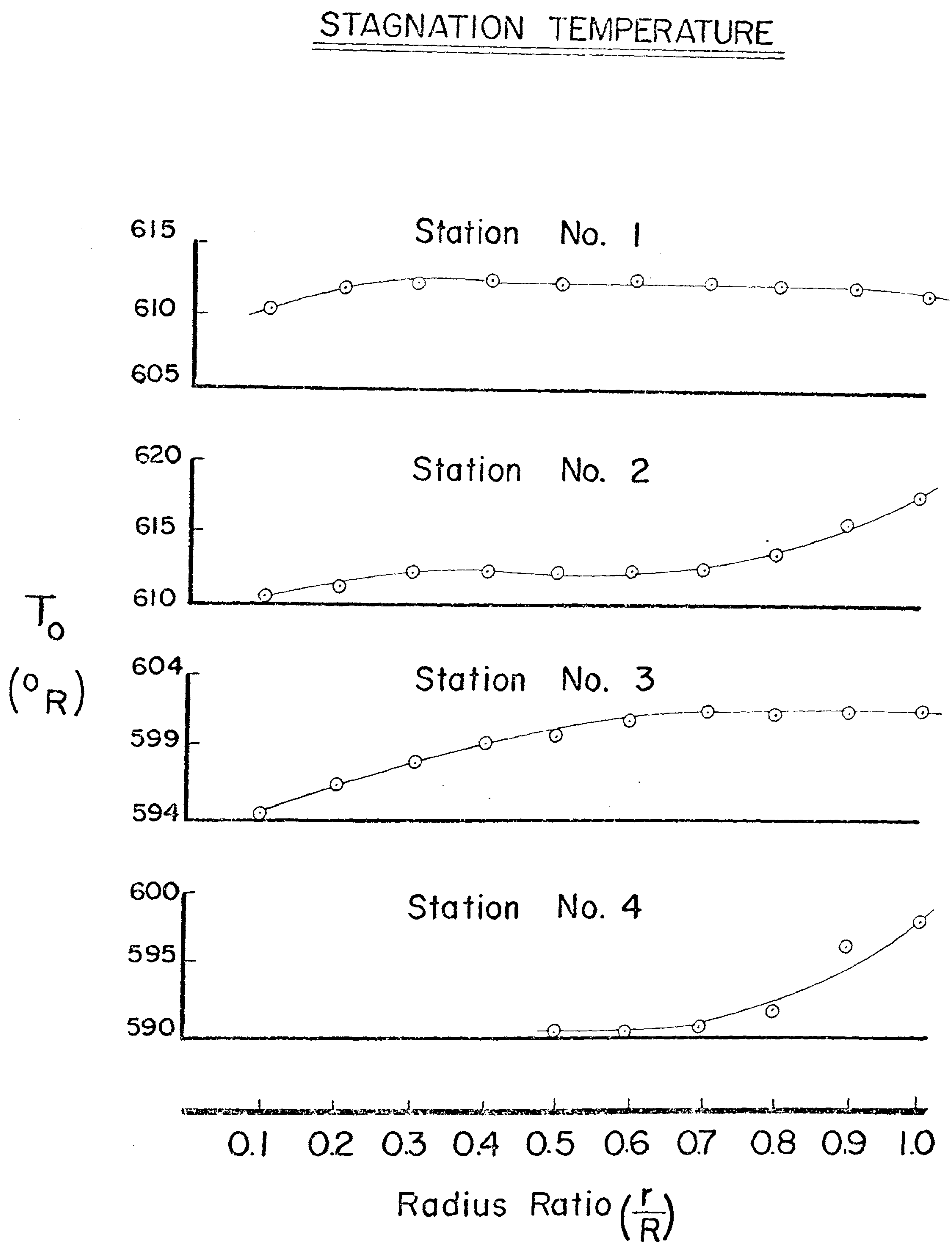

FIGURE 16. Stagnation Temperature vs. Radius Ratio

VI. ERROR ANALYSIS

Error in the experimental data can be attributed to two main factors. First of all, some flow disturbance due to the instrumentation must be acknowledged. The large nozzle and small probe served to minimize this disturbance, but since the probe and support tubes were in the flow, the error could not be completely eliminated. Secondly the oil from the Gardener-Denver compressor would tend to alter the properties of the fluid passing through the nozzle.

An attempt was made to calibrate the sensing probes. The probes were checked inside a small subsonic wind tunnel. The maximum velocity in the tunnel was fifty feet per second. At the low air speeds the probes demonstrated recovery factors of unity. Since this wind tunnel was the only means of calibration available, the recovery factors of the sensing probes were assumed equal to unity at all air speeds.

VII. CONCLUSIONS AND RECOMMENDATIONS

The conclusions gathered from the experimental study may be stated as follows:

1.) The tangential or swirl component of velocity was the largest component.

2.) The tangential velocity distribution changed from that of a frictionless or potential vortex at the entrance to that of a rotational vortex at the exit.

3.) A region of low static pressure and reversed axial flow existed in the core of the vortex.

4.) The discharge of mass was mainly from an annular region near the wall of the nozzle, with possibly some discharge in the very center of the exit plane.

5.) The radial velocity component had a magnitude which was too large to neglect.

6.) A converging nozzle tended to increase the magnitude of the axial velocity component with respect to the total velocity.

7.) The Ranque-Hilsh effect was verifed.

The following is a list of recommendations for further work of this nature.

1.) More axial stations should be constructed to allow for the collection of data at more axial positions.

2.) When a larger air supply is available, a study of variable flow rate should be made.

3.) The larger air supply will allow choking of the flow and a supersonic flow analysis.

4.) A divergent section should be added to the converging nozzle.

5.) A thorough analytical study of the flow pattern would be of value.

NOMENCLATURE

Variables

P_a = atmospheric pressure psia

P_o = local stagnation pressure psia

P_s = local static pressure psia

P_{up} = upstream pressure at orifice psia

ΔP = differential across orifice psia

ρ = local density of air lb/ft^3

$\overline{T}_a$ = atmospheric temperature ^oF

T_a = atmospheric temperature ^oR

T_o = local stagnation temperature ^oR

T_s = local static temperature ^oR

$\overline{V}$ = total velocity ft/sec

V_a = axial velocity componet ft/sec

V_r = radial velocity componet ft/sec

V_o = tangential velocity componet ft/sec

Z = axial distance from nozzle entrance in.

ΔH_a = atmospheric pressure in. of HG

ΔH = manometer reading $P_o - P_s$ in. of H_2O

Δh = manometer reading $P_a - P_s$ in. of H_2O

R = total radius in.

r = radius in.

Re = $\frac{VD\rho}{\mu}$ = Reynolds Number

Constants

A_o = orfice area = $(D_o^2/(4)(144))$ ft^2

c_p = constant pressure specific heat = .24 BTU/°R

D_o = diameter of orfice = 1.50 in.

D_p = inside diameter of primary line = 2.068 in.

g = local acceleration of gravity = 32.2 ft/sec^2

g_c = gravitional constant = 32.2 ft/sec^2

R = gas constant for air = 53.3 lb_f-ft/lb_m°R

J = proportionality factor = 778 ft-lb_f/BTU

k = ratio of specific heats for air = 1.4

ρ_w = standard density of water = 62.4 lb_m/ft^3

μ = viscosity of air = 1.35×10^{-5} lb_m/sec-ft

Angular positions of the support tubes

Refer to Figure 17.

λ = horizontal rotation of positioning sphere - degrees

β = vertical inclination of the support tubes - degrees

∇ = rotation of sensing tube with respect to the support tubes - degrees

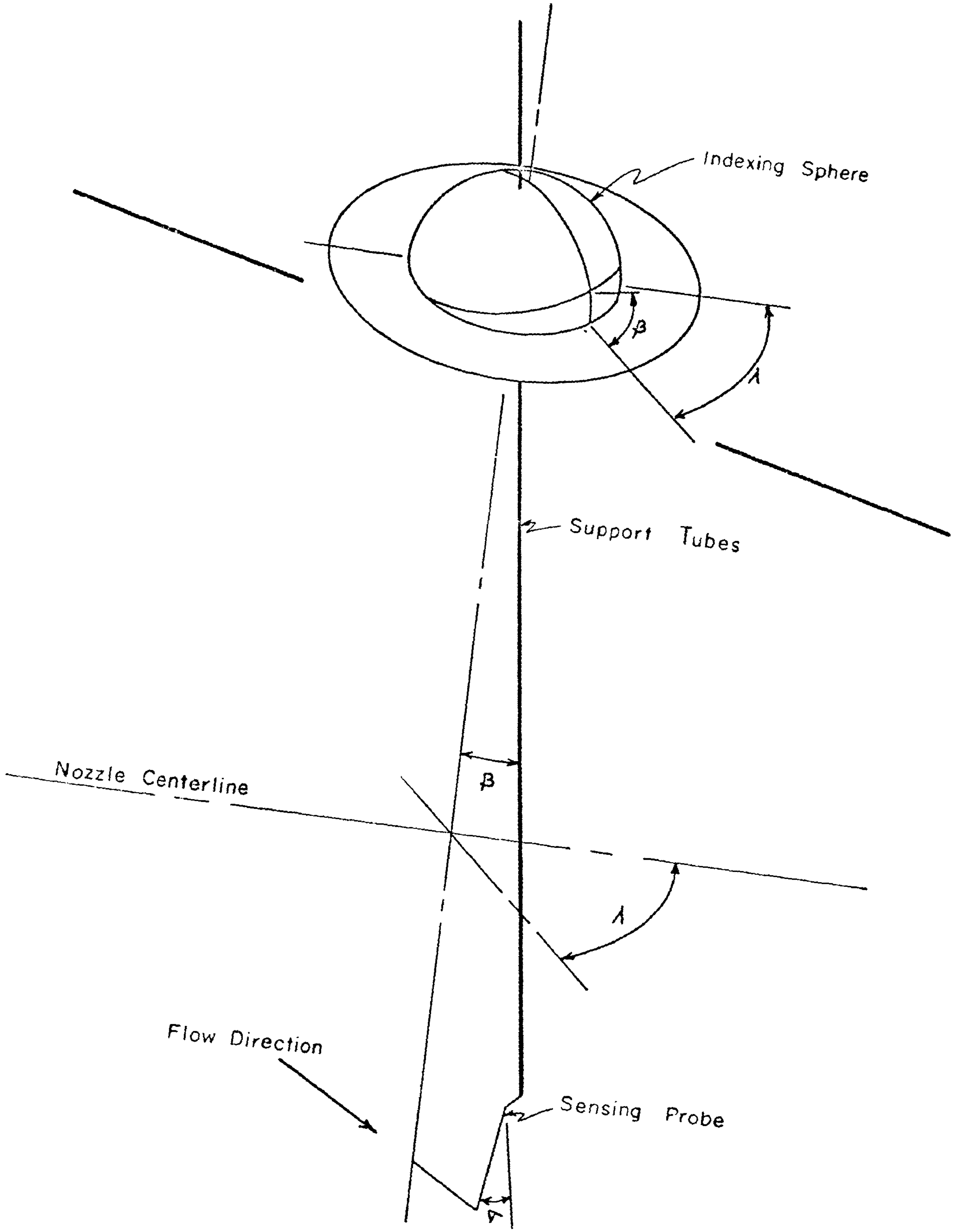

FIGURE 17. Angular Positions

APPENDIX

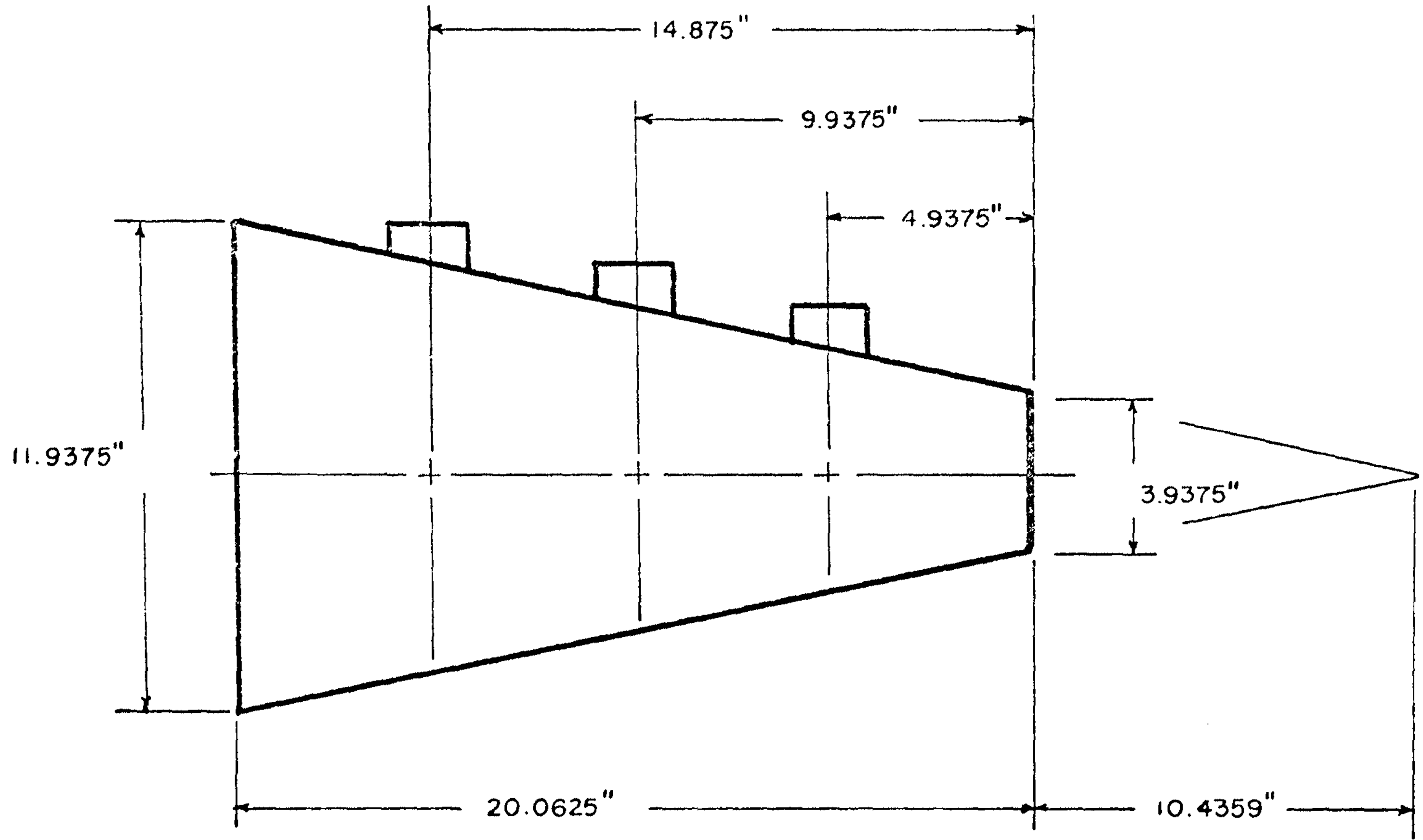

FIGURE 18. Nozzle Dimensions

TABLE I

EXPERIMENTAL DATA

Station No. 1

Z = 14.875 in.

Ambient Pressure = 29.12 in. HG

Ambient Temperature = 74° F

Receiving Tank Pressure = 3.5 psig

Inlet Air Temperature = 3.391 mv

Nozzle Surface Temperatures

T center = 3.155 mv

T exit = 3.046 mv

Orfice Data ΔP = 3.01 in. HG

P_{up} = 5.0 psig

ℓ (in.)	r/R	Sensing tube positions			Velocity (in. of H_2O)	$(P_a - P_s)$ (in. of H_2O)	T_o (mv)
		λ	β	σ			
5.35	1.0	71°	7.0°	-2.5°	1.50	-9.50	2.765
5.05	0.9	68°	7.0°	15.0°	2.25	-9.55	2.772
4.71	0.8	74°	9.5°	21.0°	2.58	-8.25	2.775
4.40	0.7	86°	8.0°	18.0°	2.95	-7.62	2.780
4.06	0.6	105°	10.0°	18.0°	3.40	-6.90	2.781
3.75	0.5	111°	12.0°	21.0°	4.31	-5.85	2.772
3.38	0.4	104°	12.0°	16.0°	4.78	-4.25	2.778
3.07	0.3	96°	10.0°	13.0°	5.05	1.45	2.775
2.74	0.2	96°	10.0°	13.0°	4.61	3.35	2.762
2.43	0.1	92°	14.0°	15.0°	2.62	5.86	2.724

TABLE I (continued)

EXPERIMENTAL DATA

Station No. 2

Z = 9.9375 in.

Ambient Pressure = 29.12 in. HG

Ambient Temperature = 74° F

Receiving Tank Pressure = 3.5 psig

Inlet Air Temperature = 3.391

Nozzle Surface Temperatures

T center = 3.155 mv

T exit = 3.046 mv

Orfice Data ΔP = 3.01 in. HG

P_{up} = 5.0 psig

ℓ (in.)	r/R	Sensing tube positions			Velocity (in. of H_2O)	$(P_a - P_s)$ (in. of H_2O)	T_o (mv)
		λ	β	σ			
5.35	1.0	73°	5.0°	-3.0°	1.96	-8.17	2.904
5.05	0.9	74°	7.0°	14.0°	2.35	-7.75	2.862
4.71	0.8	74°	9.0°	17.0°	3.00	-7.32	2.774
4.40	0.7	84°	10.0°	22.0°	3.40	-6.52	2.772
4.06	0.6	98°	10.0°	20.0°	3.85	-4.87	2.766
3.75	0.5	110°	11.0°	28.0°	4.40	-2.98	2.762
3.38	0.4	102°	11.0°	28.0°	4.95	-2.05	2.765
3.07	0.3	104°	13.0°	26.0°	4.90	0.0	2.760
2.74	0.2	93°	11.0°	27.0°	4.20	2.60	2.736
2.43	0.1	91°	11.0°	24.0°	3.10	5.56	2.719

TABLE I (continued)

EXPERIMENTAL DATA

Station No. 3

Z = 4.9375

Ambient Pressure = 27.70 in. HG

Ambient Temperature = 71° F

Receiving Tank Pressure = 3.0 psig

Inlet Air Temperature = 3.271 mv

Nozzle Surface Temperatures

T center = 3.041 mv

T exit = 2.912 mv

Orfice Data ΔP = 3.05 in. HG

P_{up} = 5.17 psig

ℓ (in.)	r/R	Sensing tube positions			Velocity (in. of H_2O)	$(P_a - P_s)$ (in. of H_2O)	T_o (mv)
		λ	β	σ			
5.35	1.0	56°	11.0°	7.0°	3.42	-6.35	2.503
5.05	0.9	75°	10.0°	14.0°	4.75	-6.20	2.500
4.71	0.8	91°	13.0°	17.0°	5.50	-4.75	2.495
4.40	0.7	93°	14.0°	20.5°	5.92	-2.65	2.491
4.06	0.6	91°	15.0°	21.5°	6.05	-1.35	2.480
3.75	0.5	98°	15.5°	18.0°	6.20	1.05	2.464
3.38	0.4	92°	13.0°	17.0°	5.75	2.63	2.448
3.07	0.3	88°	14.0°	18.0°	4.47	4.15	2.405
2.74	0.2	85°	15.0°	20.5°	2.60	7.05	2.372
2.43	0.1	84°	15.0°	22.0°	2.02	8.55	2.335

TABLE I (continued)

EXPERIMENTAL DATA

Station No. 4

Z = 0.0

Ambient Pressure = 28.70 in. HG

Ambient Temperature = 71° F

Receiving Tank Pressure = 3.0 psig

Inlet Air Temperature = 3.270 mv

Nozzle Surface Temperatures

T center = 3.040 mv

T exit = 2.912 mv

Orfice Data Δ P = 3.05 in. HG

P_{up} = 5.17 psig

ℓ (in.)	r/R	Sensing tube positions			Velocity (in. of H_2O)	$(P_a - P_s)$ (in. of H_2O)	T_o (mv)
		λ	β	σ			
5.35	1.0	43°	2.0°	-1.0°	12.19	-0.95	2.425
5.05	0.9	52°	2.0°	-2.0°	8.65	2.40	2.380
4.71	0.8	72°	3.0°	14.0°	5.14	2.62	2.276
4.40	0.7	87°	3.0°	16.0°	3.20	3.17	2.250
4.06	0.6	100°	5.0°	22.0°	1.45	3.85	2.235
3.75	0.5	93°	6.0°	22.5°	0.85	4.67	2.234
3.38	0.4	--	--	--	--	--	--
3.07	0.3	--	--	--	--	--	--
2.74	0.2	--	--	--	--	--	--
2,43	0.1	--	--	--	--	--	--

TABLE II

CALCULATED DATA

Station No. 1 - Z/L = 0.495

Ambient Pressure = 14.29 psia

Ambient Temperature = 534.0° R

Receiving Tank Pressure = 17.59 psia

Inlet Air Temperature = 609.3° R

Mass Flowrate = 0.2827 lb_m/sec

Volumetric Flowrate = 198.3 ft^3/min

Nozzle Surface Temperatures

T center = 601.3° R

T exit = 597.3° R

Orfice Data ΔP = 1.478 psia

P_{up} = 19.29 psia

r/R	P_s/P_a	T_o (°R)	T_s (°R)	ρ lb/ft^3	Angles		Velocities (ft. per sec.)			
					ψ	ϕ	V	V_θ	V_r	V_a
1.0	1.024	611.86	611.21	.0646	71°	-9.5°	88.20	82.26	-14.55	28.35
0.9	1.022	612.10	611.21	.0645	68°	8.0°	108.19	99.29	15.04	40.06
0.8	1.021	612.20	611.10	.0644	74°	10.5°	115.76	109.35	21.07	31.41
0.7	1.019	612.38	611.09	.0643	86°	11.0°	124.09	121.49	23.70	8.42
0.6	1.017	612.41	610.94	.0642	105°	8.0°	133.04	127.23	18.49	-34.11
0.5	1.015	612.10	609.12	.0643	111°	9.0°	149.97	138.25	23.39	-52.99
0.4	1.011	612.31	610.24	.0639	104°	4.0°	158.43	153.21	10.93	-38.07
0.3	0.996	612.20	609.94	.0630	96°	3.0°	163.71	162.56	8.51	-17.15
0.2	0.992	611.76	609.68	.0627	96°	3.0°	156.84	155.75	8.10	-16.45
0.1	0.985	610.21	609.94	.0633	92°	1.0°	118.74	118.50	2.80	-4.15

TABLE II (continued)

CALCULATED DATA

Station No. 2 - Z/L = 0.495

Ambient Pressure = 14.29 psia

Ambient Temperature = 534.0° R

Receiving Tank Pressure = 17.59 psia

Inlet Air Temperature = 609.3° R

Mass Flowrate = 0.2827 lb_m/sec

Volumetric Flowrate = 198.3 ft^3/min

Nozzle Surface Temperatures

T center = 601.3° R

T exit = 597.3° R

Orfice Data ΔP = 1.478 psia

P_{up} = 19.29 psia

r/R	P_s/P_a	T_o (°R)	T_s (°R)	ρ lb/ft³	Angles ψ	Angles ϕ	Velocities (ft. per sec.) V	V_θ	V_r	V_a
1.0	1.021	617.80	616.94	.0638	73°	-9.0°	100.99	95.29	-15.75	29.10
0.9	1.020	616.12	614.89	.0640	74°	7.0°	122.06	116.48	14.89	32.03
0.8	1.019	612.48	611.19	.0643	74°	7.0°	124.90	119.19	15.24	32.78
0.7	1.016	612.41	610.94	.0642	84°	11.0°	133.04	129.73	25.41	13.70
0.6	1.012	612.21	610.56	.0640	98°	9.0°	142.13	138.88	22.17	-19.40
0.5	1.008	612.17	610.12	.0624	110°	16.0°	153.62	138.62	42.25	-50.49
0.4	1.005	612.07	609.96	.0636	102°	16.0°	161.55	151.83	44.43	-32.29
0.3	1.000	612.00	609.87	.0632	104°	12.0°	160.93	152.67	33.47	-38.09
0.2	0.993	611.02	609.11	.0629	93°	15.0°	149.67	144.14	38.61	-7.55
0.1	0.986	610.32	608.92	.0625	91°	12.0°	128.84	125.88	26.79	-2.20

TABLE II (continued)

CALCULATED DATA

Station No. 3 - Z/L 0.239

Ambient Pressure = 14.09 psia

Ambient Temperature = 531.0° R

Receiving Tank Pressure = 17.09 psia

Inlet Air Temperature = 597.6° R

Mass Flowrate = 0.2870 lb_m/sec

Volumetric Flowrate = 201.2 ft^3/min

Nozzle Surface Temperatures

T center = 591.6° R

T exit = 586.6° R

Orfice Data ΔP = 1.497 psia

P_{up} = 19.26 psia

r/R	P_s/P_a	T_o ($^{\circ}R$)	T_s ($^{\circ}R$)	ρ lb/ft^3	Angles		Velocities (ft. per sec.)			
					ψ	ϕ	$\bar{V}$	V_θ	V_r	V_a
1.0	1.016	601.63	600.16	.0644	56°	-4.0°	133.42	110.27	-9.29	74.36
0.9	1.016	601.54	599.50	.0645	74°	2.0°	134.16	128.80	4.69	36.86
0.8	1.014	601.04	598.66	.0643	91°	2.0°	169.17	168.83	5.90	-2.96
0.7	1.007	601.03	598.45	.0640	93°	3.5°	176.07	175.36	10.75	-9.19
0.6	1.004	600.93	598.29	.0638	91°	4.5°	178.33	177.61	12.39	-3.11
0.5	0.997	599.87	597.12	.0635	98°	1.5°	180.83	178.84	3.16	-25.15
0.4	0.994	599.21	596.70	.0633	92°	2.0°	174.35	174.00	6.08	-6.08
0.3	0.987	597.47	595.50	.0632	88°	2.0°	153.95	153.63	5.37	5.37
0.2	0.981	596.08	594.95	.0627	85°	3.5°	117.89	117.13	7.19	7.19
0.1	0.978	594.47	593.58	.0627	84°	5.0°	103.92	103.92	9.05	10.82

TABLE II (continued)

CALCULATED DATA

Station No. 4 - Z/L = 0.0

Ambient Pressure = 14.09 psia

Ambient Temperature = 531.0° R

Receiving Tank Pressure = 17.09 psia

Inlet Air Temperature = 597.6° R

Mass Flowrate = 0.2870 lb_m/sec

Volumetric Flowrate = 201.2 ft^3/min.

Nozzle Surface Temperatures

T center = 591.6° R

T exit = 586.6° R

Orfice Data ΔP = 1.497 psia

P_{up} = 19.26 psia

r/R	P_s/P_a	T_s (°R)	T_o (°R)	lb/ft^3	Angles		Velocities (ft. per sec.)			
					ψ	ϕ	$\bar{V}$	V_θ	V_r	V_z
1.0	1.002	597.97	592.69	.0643	43°	-9.0°	251.99	182.00	-39.31	169.80
0.9	0.994	596.11	592.32	.0640	52°	-10.0°	213.07	165.38	-36.86	129.07
0.8	0.993	591.78	589.54	.0641	72°	5.0°	164.01	152.07	14.27	50.48
0.7	0.992	590.69	589.28	.0640	87°	7.0°	129.23	128.06	15.77	6.67
0.6	0.990	590.07	589.48	.0640	100°	11.0°	87.18	84.32	16.56	-14.89
0.5	0.988	590.02	589.65	.0637	93°	10.5°	67.08	65.81	12.21	-3.43
0.4	--	--	--	--	--	--	--	--	--	--
0.3	--	--	--	--	--	--	--	--	--	--
0.2	--	--	--	--	--	--	--	--	--	--
0.1	--	--	--	--	--	--	--	--	--	--

SAMPLE CALCULATIONS

Sample calculations are performed for station one, at $r/R = 0.6$. In all calculations, air is assumed to be a perfect gas.

(1.) Calculations for atmospheric conditions.

$$P_a = (\Delta H_a)(0.491 \text{ psia/in. of HG})$$

$$T_a = \overline{T}_a + 460^\circ \text{ R}$$

Sample: $P_a = (29.12)(0.491) = 14.297$ psia

$$T_a = 74 + 460 = 534^\circ \text{ R}$$

(2.) Calculations for static pressure.

Since: $P_a - P_s = \dfrac{(\Delta h)(\rho w)}{(12)(144)}$

Therefore: $P_s = P_a - \dfrac{(\Delta h)(\rho w)}{(12)(144)}$

Sample: $P_s = 14.297 - \dfrac{(-6.90)(62.4)}{(12)(144)} = 14.564$ psia

(3.) Calculations for static temperature:

[1] $c_p T_o = c_p T_s + \dfrac{V^2}{2 g_c J}$ (energy equation)

[2] $V = \sqrt{\dfrac{2 g_c}{\rho}(P_o - P_s)(144)}$

substituting eq.2 into eq. 1 yields,

[3] $c_p T_o = c_p T_s + \dfrac{\dfrac{2 g_c}{\rho}(P_o - P_s)(144)}{2 g_c J}$

and for an ideal gas,

[4] $\rho = \dfrac{P_s(144)}{R T_s}$

substituting eq. 4 into eq. 3 yields,

$$[5] \quad c_pT_o = c_pT_s + \frac{2rc(P_o - P_s)(144)}{J[P_s(144)/RT_s](2g_c)}$$

solving eq. 5 for T_s yields,

$$[6] \quad T_s = \frac{T_o}{1.0 + \left[\frac{R}{c_pJ}\frac{(P_o - P_s)}{(P_s)}\right]}$$

Sample:

$$T_s = \frac{612.41}{\left[1.0 + \frac{(53.3)}{(.24)(778)} \frac{\frac{3.40}{(12)}(62.4)(1/144)}{14.546}\right]}$$

$$T_s = 610.94^o\ R$$

(4.) Calculation of densities.

assuming air to be an ideal gas,

$$[4] \quad \rho = \frac{P_s(144)}{RT_s}$$

Sample:

$$\rho = \frac{(14.546)(144)}{(53.3)(610.94)} = 0.0643\ lb/ft^3$$

(5.) Calculation of total velocities.

$$[2] \quad \overline{V} = \sqrt{\frac{2g_c}{\rho}(P_o - P_s)(144)}$$

Sample:

$$\overline{V} = \sqrt{\frac{(2)(32.2)}{(0.06434)}\frac{(3.40)(62.4)}{(12)}} = 133.04\ ft/sec$$

(6.) Calculations for resolving the total velocities into components, Figure (19).

The direction of the velocity vector at a data point can be obtained from the angles λ, β, and Γ. The geometry of the system is related as follows:

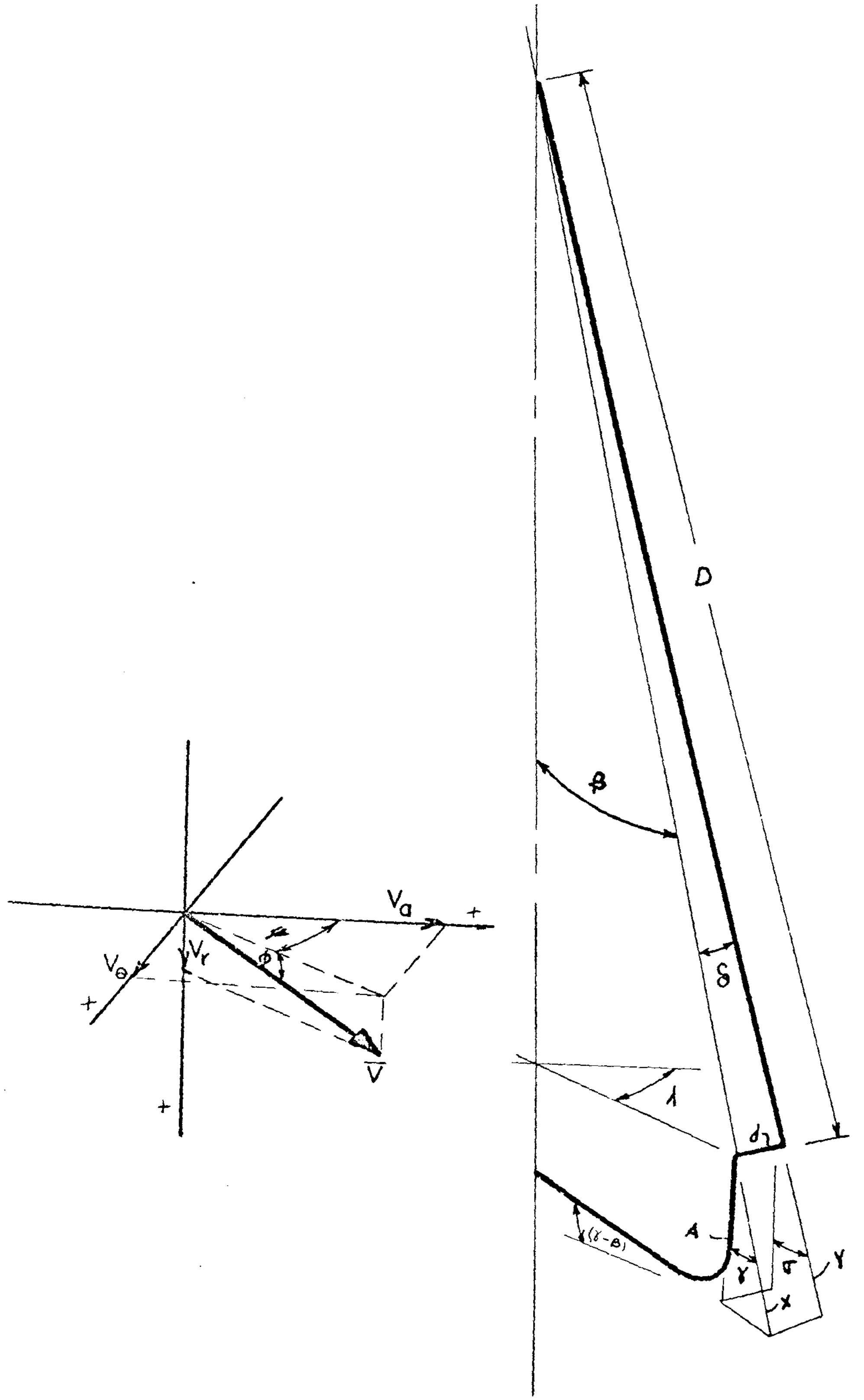

FIGURE 19. Geometry of Support Mechanism

$$\tau = \cos^{-1}\frac{A}{Y} \qquad \cos\tau = \frac{A}{Y}$$

$$\gamma = \cos^{-1}\frac{A}{X} \qquad \cos\gamma = \frac{A}{Y}$$

$$\delta = \cos^{-1}\frac{Y}{X} \qquad \cos\delta = \frac{Y}{X}$$

And: $\frac{A}{X} = \frac{A}{Y}\,\frac{Y}{X}$

Therefore: $\cos\gamma = (\cos\tau)(\cos\delta)$

and since $\delta = \tan^{-1}\frac{d}{D}$, δ can be obtained.

The worst possible condition (i.e. the largest δ) would occur at station three in the center of the nozzle. At this position,

$D = 4.56$ in.

$d = 0.75$ in.

so, $\tan\delta = \frac{0.75}{4.56} = 0.164$

and, $\delta = 9.5^{\circ}$

Then for this position $\cos\gamma = \cos\tau(.987)$.

The above analysis indicates that the assumption $\tau = \gamma$ does not introduce appreciable error. With this assumption the spherical coordinates of the velocity are as follows:

$\psi = \lambda$

$\phi = (\tau - \beta)$

With these coordinates, the velocity components can be calculated.

$V_r = \overline{V} \sin\phi$

$V_a = \overline{V} \cos\phi \cos\psi$

$V_\theta = \overline{V} \cos\phi \sin\psi$

Sample:

$\psi = 105^\circ$

$\phi = (18^\circ - 10^\circ) = 8^\circ$

$V_r = (133.04)(\sin 8^\circ) = 18.49$ ft/sec

$V_a = (133.04)(\cos 8^\circ)(\cos 105^\circ) = -34.11$ ft/sec

$V_\theta = (133.04)(\cos 8^\circ)(\sin 105^\circ) = 127.23$ ft/sec

(7.) Calculations for laser positions.

To shine the laser beam through a desired point inside the nozzle, it was necessary to pivot the beam through a specific angle, corresponding to the desired point. The points of interest at each station were located at radius ratios of .1, .2, .3, .4, ... 1.0. Since the beam was pivoted about a point corresponding to the apex of the nozzle, the beam position for a particular radius ratio at station one, was also the position for that same radius ratio at station two, or any other axial station. This can be shown, by considering two different stations along the nozzle axis, Figure 20.

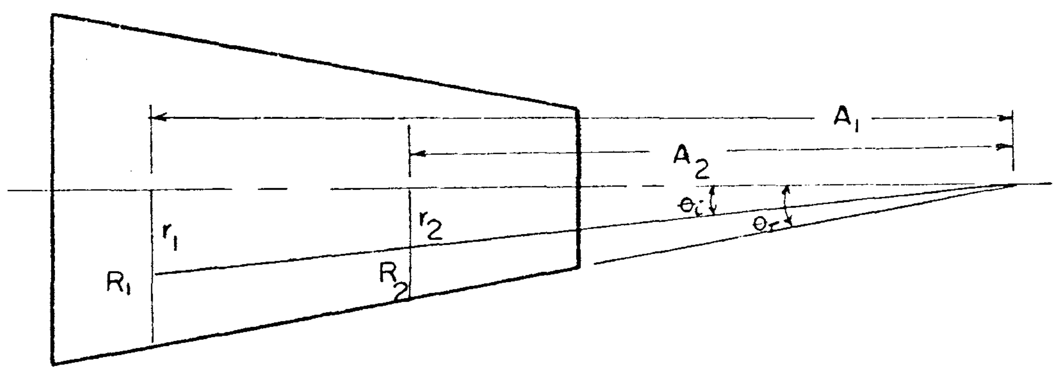

FIGURE 20. Beam Geometry for Two Axial Stations

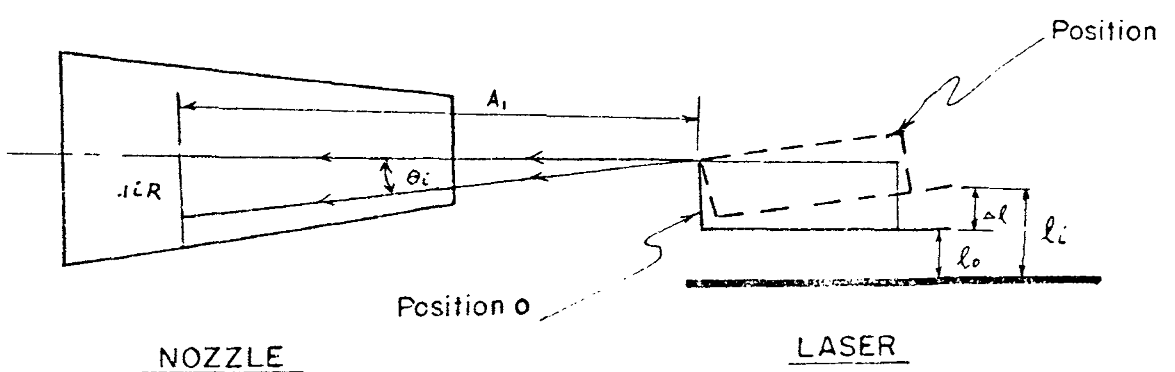

FIGURE 21. Beam Geometry for a Single Station

$$\tan \theta_t = \frac{R_1}{A_1} = \frac{R_2}{A_2} \quad ; \quad A_2 = A_1 \frac{R_2}{R_1}$$

$$\tan \theta_i = \frac{r_1}{A_1} = \frac{r_2}{A_2}$$

$r_1 = mR_1$

$r_2 = nR_2$ where m and n are fractions less than 1.0

$$\tan \theta_i = \frac{mR_1}{A_1} = \frac{nR_2}{A_2}$$

substituting for A_2;

$$\frac{mR_2}{\frac{R_2}{R_1}A_1} = \frac{nR_1}{A_1}$$

this yields m = n, so the angle θ_i is the same for corresponding radius ratios at different stations.

The values of θ_i were calculated as shown below, for values of radius ratio from .1 to 1.0. These values are tabulated in table 3. (Figure 21) $\tan \theta_i = 0.1(i)R/A$

For the ten desired radius ratios the subscript i takes on values of 1 through 10, in increments of 1. They were calculated using the dimensions of station one.

Sample: $r = (.1)i(R)$

$$\tan \theta_6 = \frac{0.1(6)(4.95)}{25.31} = 0.1173$$

$$\theta_6 = \mathrm{Tan}^{-1}\ 0.1173 = 6.7^\circ$$

The ten positions of the laser were laid off using the related distance ℓ_i. ℓ_i corresponds to the distance of a point on the laser support from a reference surface. This distance is calculated by considering the geometry of the laser table, Figure (22). The values of ℓ_i are listed in table 3.

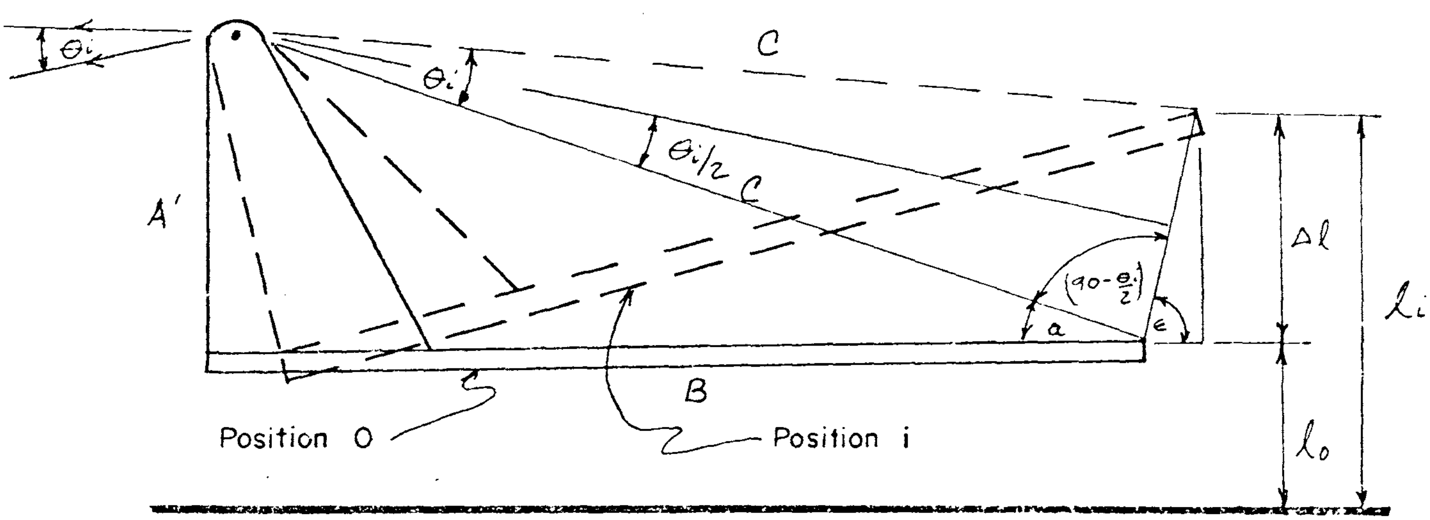

FIGURE 22. Geometry of Laser Support

$$\epsilon = 180 - (90 - \theta_i/2) - a = (90 - a + \theta_i/2)$$

$$D' = 2C\sin \theta_i/2$$

$$\Delta\ell = D'\sin(\epsilon) = 2C\sin \theta_i/2 \ (\sin\epsilon)$$

$$\ell_i = \ell_o + \Delta\ell$$

Sample:

$$a = \tan^{-1} 3.5/16.7 = 0.2095$$

$$a = 11.8^\circ$$

$$\epsilon = 90 - a + \theta_6/2$$

$$\epsilon = 90 - 11.8 - 3.35 = 74.85^\circ$$

$$C = \sqrt{(3.5)^2 + (16.7)^2} = 17.06 \text{ in.}$$

$$\Delta \ell = 2(17.06) \sin (6.7/2) \sin (74.85)$$

$$\Delta \ell = 34.12(0.058)(0.965) = 1.956 \text{ in.}$$

$$\ell_i = 2.10 + 1.956 = 4.056 \text{ in.}$$

TABLE III

LASER POSITIONS

i	1	2	3	4	5	6	7	8	9	10
r/R	.1	.2	.3	.4	.5	.6	.7	.8	.9	1.0
θ_i°	1.1	2.2	3.4	4.5	5.58	6.7	7.8	8.9	10.0	11.0
in.	2.43	2.74	3.07	3.38	3.75	4.06	4.40	4.71	5.05	5.35

(8.) Calculations for flowrate.

The coefficient of discharge of the orifice was calculated using a relationship given by the ASME.

$$C_d = K(1.0 - B^4)^{\frac{1}{2}}$$

where, C_d = coefficient of discharge

$$B = D_o/D_p$$

$$K = K_0(1.0 + B\ E/Re)$$

with,

$$E = D_o(830 - 5000B + 9000B^2 - 4200B^3 + 530/D_p^{\frac{1}{2}}$$

$$Ke = 0.5993 + 0.007/D_p^2 + (0.364 + 0.076/D_p^{\frac{1}{2}})B^4 + (65/D_p^2 + 3.0)(B - 0.7)^{5/2}$$

$$K_0 = K_e(10^6)(D_o)/(10^6 D_o + 15E)$$

From the definition of the discharge coefficient $W_a = C_d\ W_t$. Where W_a is the actual mass flowrate and W_t is the theoretical flowrate.

As shown by Benedict (2), the theoretical flowrate can be obtained from the following relationship.

$$W_t = \rho_2 A_2 V_2$$

$$W_t = A_2 \left[\frac{(2k/k-1)(1 - (P_2/P_1)^{\frac{k-1}{k}})\ P_1 g \rho_1\ (P_2/P_1)^{\frac{2}{k}}}{(1 - (P_2/P_1)^{\frac{2}{k}}\ B^4)} \right]^{\frac{1}{2}}$$

where the subscript 1 refers to the upstream conditions, and the subscript 2 refers to the downstream conditions.

This equation yields the theoretical flowrate, but the solution for the actual flowrate requires an iteration process because both the coefficient of discharge and the actual flowrate are functions of Reynolds number.

A copy of the computer program used to complete the iteration process is shown below. The computer language is Fortran IV.

Computer Nomenclature: PD = D_p , OD = D_o , Re = inital Re

Q = k , C = μ , R = R

G = g_c ,PIE = π , P1 = P_{up}

DP= P , TA = T_a , PA = P_a

```
      READ (1,100) PD,OD,RE,Q,C,R
      READ(1,100)G,PIE,P1,DP,TA,PA
      P1=P1+PA
      B= OD/ PD
      P2=P1-DP
      P1=P1*144.0
      P2=P2*144.0
      RO1=(P1/(R*TA))
      A=(2.0*Q/(Q-1.0))
      AB= (Q-1.0)/Q
      AC=   (2.0/Q)
      AO=(PIE*OD**2.0)/(4.0*144.0)
      WT1=AO*(A*(1.0-(P2/P1)**AB)*P1*G*RO1*(P2/P1)**AC) * *.5
      WT2 = (1.0 -(P2/P1)**AC * B**4.0) ** .5
      WT= WT1/WT2
      E=(830.0-5000.0*B+9000.0*B**2.0-4200.0*B**3.0+530.0/(PD**.5))*OD
      QN=  0.5993 +0.007/PD +(0.364 +0.076/ PD**.5 )*B**4.0
      QM=(65.0/PD**2.0+3.0)*((B-0.7)**2.5)
      QE= QN+QM
      QO=((QE*10.0**6.0)*OD)/((10.0**6.0)*OD+15.0*E)
      WRITE(3,300)RO1,B,P1,P2,AO
      WRITE(3,300)QN,QM,QO,E,WT
      DO 20 I=1,100
      QL= QO*(1.0+B*E/RE)
      CD=QL*(1.0-B**4.0 )**.5
      WA=WT *CD
      REC=(4.0*12.0*WA*G)/(PD*PIE*C*G)
      IF(ABS(REC-RE)-.25)2,2,1
    1 RE =RE + (REC-RE)/ 2.0
   20 CONTINUE
    2 WRITE (3,200)  WA,CD,REC,RE
      STOP
```

Sample:

$$B = 1.50/2.068 = 0.725$$

$$T_1 = 149.3 + 460 = 609.3^o\ R$$

$$P_1 = 5.00 + 14.29 = 19.29 \text{ psia}$$

$$P_2 = P_1 - P = 15.29 - 1.478 = 13.812 \text{ psia}$$

$$\rho_1 = P_1(144)/RT_1 = (15.29)(144)/(53.3)(609.3)$$

$$\rho_1 = 0.06779$$

$$A_2 = (3.14)(1.50)/(4)(144) = 0.01227 \text{ ft}^2$$

$$P_2/P_1 = (13.812)/(15.29) = 0.903$$

$$W_t = .01227 \left[\frac{(7)(1- 0.903^{(.286)})(19.29)(32.2)}{1 - 0.903^{(.15)}} \cdot \frac{(.06779)(.903)^{(.15)}}{(1.500)^4} \right]^{\frac{1}{2}}$$

$$W_t = 0.46 \text{ lb}_m/\text{sec}$$

$$E = 1.50(830 - 5000(0.725) + 9000\ (0.725)^2 - 4200(0.725)^3 + 530/(2.068)^{\frac{1}{2}}) = 1057.0$$

$$K_e = 0.5993 + 0.007/2.068 + (0.364 + 0.076/(2.068)^{\frac{1}{2}})(0.725)^4 + (65/(2.068)^2 + 3)(0.725 - 0.7)^{5/2} = 0.720$$

$$K_o = 0.720(10^6)(1.50)/(10^6 \times 1.50 + 15 \times 1.507 \times 10^3) = 0.713$$

After evaluating these constants, the iteration process is carried out as follows:

1. Assuming an initial value of RE = 2.0×10^5, the corresponding value of K is calculated.

$K = 0.713\ (1 + 0.725(.057 \times 10^3)/2.0 \times 10^5) =$

0.716

and

$C_d = 0.716(1 - (0.725)^4)^{\frac{1}{2}} = 0.609$

so, $W_a = 0.609(0.46) = 0.2801\ lb_m/sec$

2. The Reynolds Number corresponding to the actual flowrate is,

$$Re_c = \frac{4(W_a)(g_c)}{(D_p)\mu(g)} = \frac{(4)(.2801)(32.2)(12)}{(2.068)(3.14)(1.35\times10^{-5})\ 32.2}$$

$Re_c = 1.5336 \times 10^5$

3. Since this value does not correspond to the assumed value, the iteration must continue. To continue the process, change the value of the initially assumed Reynolds Number as follows; $RE = RE + \frac{1}{2}(RE_c - RE)$. Changing the value in this manner will reduce or increase it depending on which is necessary to bring the assumed value and the calculated value together. Therefore;

$RE = 2.0 \times 10^5 + \frac{1}{2}(1.5336 \times 10^5 - 2.0 \times 10^5)$

$RE = 2.0 \times 10^5 - .2332 \times 10^5 = 1.7668 \times 10^5$

4. Repeat steps one through three, using the corrected value of Reynolds Number for the inital value.

This procedure is repeated until the Reynolds number converges to a single value. The computer program employed to solve this problem iterated until the two values of Reynolds number differed by 0.25 or less.

The Volumetric flowrate is calculated using the relationship $Q = W_a (1/\rho)(g/gc)(60 \text{ sec./min.})$.

$\rho = P_{up} (144)/RT = 19.29(144)/(53.3)(609.3)$

$\rho = 0.08553 \ lb_m/ft^3$

Sample:

$Q = (0.2827)(1/0.08553)(32.2/32.2)(60)$

$Q = 198.3 \ ft^3/min$

(10.) Intergration of the Axial Velocity Distribution at the exit plane.

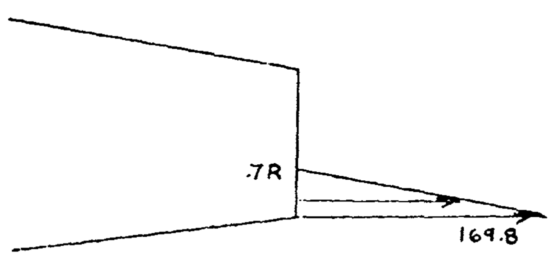

The velocity distribution is practically linear in the region of interest.

The defining equation is $V = \frac{V_{max}}{(R - .7R)}(r - .7R)$.

Continuity equation, mass flowrate $= \int_A \rho V dA$

For an annular region $dA = 2\pi r dr$.

The density is assumed constant and equal to 0.0640 lb_m/ft^3.

Therefore:

$$\dot{m} = \int_{.7R}^{R} \frac{V_{max}}{(R - .7R)} (r - .7R) 2\pi r dr$$

$$V_{max} = 169.8 \text{ ft/sec}$$

$$R = (1.95/12) = 0.1625 \text{ ft}$$

Integrating the above expression yields,

$$\dot{m} = \frac{(0.0640)(169.8)\pi(2)}{.3 R} \left[\frac{r^3}{3} - \frac{.7Rr^2}{2} \right]_{.7R}^{R}$$

$$\dot{m} = 0.247 \text{ } lb_m/sec$$

BIBLIOGRAPHY

1. Ambrosius, E. E. and Fellows, R. D., Mechanical Engineering Laboratory Practice. The Ronald Press Company, New York, N. Y., 1957, pp. 206-220.

2. Benedict, R. P., "Fluid Flow Measurement," Electro-Technology, January, 1961, pp. 55-68.

3. Binnie, A. M., Hooking, G. A. and Kamel, M. Y. M., "The Flow of Swirling Water Through a Convergent-Divergent Nozzle," Journal of Fluid Mechanics, Vol. 3, No. 3, December, 1957, pp. 261-274.

4. Deissler, R. G. and Perlmutter, M., "Analysis of the Flow and Energy Separation in a Turbulent Vortex," International Journal of Heat and Mass Transfer, Vol. 1-2, 1960-1961, pp. 173-191.

5. Donaldson, C. du P. and Sullivan, R. D., "Behavior of Solutions of the Navier-Stokes Equations for a Complete Class of Three-Dimensional Viscous Vortices," Proceedings of the Heat Transfer and Fluid Mechanics Institute, Stanford University, California, June, 1960, pp. 16-30.

6. Hilsch, R., "The Use of the Expansion of Gases in a Centrifugal Field as a Cooling Process," The Review of Scientific Instruments, Bol. 18, No.2, February, 1947, pp. 108-113.

7. Keyes, J. J., "An Experimental Study of Gas Dynamics in High Velocity Vortex Flow," Proceedings of the Heat Transfer and Fluid Mechanics Institute, Stanford University, California, June, 1960, pp. 31-46.

8. Lay, J. E., "An Experimental and Analytical Study of Vortex-Flow Temperature Separation by Superposition of Spiral and Axial Flows, Parts 1 and 2," Journal of Heat Transfer, Transactions ASME, Series C, Vol. 81, August, 1959; Part 1: pp. 202-212; Part 2: pp. 213-222.

9. Mager, A., "Approximate Solution of Isentropic Swirling Flow Through a Nozzle," ARS Journal, Vol. 31, No. 8, August, 1961, pp. 1140-1148.

10. Reynolds, A. J., "A Note on Vortex-Tube Flows," Journal of Fluid Mechanics, 1962, pp. 18-20

11. Savino, J. M. and Ragsdale, R. G., "Some Temperature and Pressure Measurements in Confined Vortex Fields," Journal of Heat Transfer, Transactions ASME, Series C, Vol. 83, No. 1, February, 1961, pp. 33-38.

12. Shapiro, A. J., The Dynamics and Thermodynamics of Compressible Fluid Flow. The Ronald Press Company, New York, N. Y., Vol. 1, 1953, and Vol. 2, 1954; Vol. 1: pp. 265-297; Vol. 2: pp. 774-783.

13. Thompson, S. A., (1966), "Measurement of the Velocity and Temperature Profiles of Air Swirling Through a Conical Shaped Nozzle." Thesis, University of Missouri at Rolla, 1966, 41 pp., (with 16 figures, 2 tables.)

VITA

The author was born in Marceline, Missouri, on July 11, 1944. His parents are Thomas S. and Cecilia A. Lineberry, both natives of north Missouri.

He received a primary education at St. Bonaventure parochial school and a secondary education at the Marceline city high school.

Upon completion of high school in May 1962, he entered the University of Missouri School of Mines and Metallurgy at Rolla, Missouri, the following September. On January 30, 1965, he was married to the former Miss Jane L. Hayes, also of Marceline, Missouri.

In August, 1966, he received a Bachelor of Science degree in Mechanical Engineering from the University, and was granted a Graduate Assistantship in the Department of Engineering Technology. The following September he enrolled in the Graduate School of the Mechanical Engineering Department.